

MULTI-CHANNEL ESTIMATE OF THE SEISMIC WAVELET

A Thesis
Presented to the
Graduate Faculty of the
College of Natural Sciences and Mathematics
University of Houston

In Partial Fulfillment
of the Requirements for the Degree
Master of Science

by
Jose Eduardo Thomas

December, 1976

MULTI-CHANNEL ESTIMATE OF THE SEISMIC WAVELET

Abstract
of a Thesis
Presented to the
Graduate Faculty of the
College of Natural Sciences and Mathematics
University of Houston

In Partial Fulfillment
Of the Requirements for the Degree
Master of Sciences

by

Jose Eduardo Thomas

December, 1976

ABSTRACT

In the stochastic deconvolution process, the assumption of a random reflectivity function can be replaced by the NMO curve and a CDP gather record. With this information, the seismic wavelet can be compressed. This compression method operates in a manner opposite to the NMO correction stretch. Shaping filters are iteratively computed either in the time domain or in the frequency domain which subsequently compress the seismic wavelet.

Based on the principle of the wavelet compression technique, the seismic wavelet can be extracted without making any assumption about the shape of the seismic wavelet. From an initial estimate of the seismic wavelet, the method computes iteratively new estimates of the seismic wavelet by minimizing the energy error between the predicted seismic trace at various offsets and the field traces at the same offsets. The NMO-curve provides the information to predict the far traces from the near traces. Stability problems limit the process to wideband source signatures.

TABLE OF CONTENTS

	Page
ACKNOWLEDGEMENTS	vii
LIST OF FIGURES	viii
INTRODUCTION	1
STRUCTURE OF THE FIELD RECORD	3
WAVELET COMPRESSION TECHNIQUE	10
Frequency Domain	10
An Isolated Spike Case	15
Synthetic Seismogram	16
Time Domain	18
An Isolated Spike Case	19
Synthetic Seismogram	20
WAVELET EXTRACTION TECHNIQUE	22
Two Point Minimum-Delay Wavelet	27
Two Point Maximum-Delay Wavelet	30
Three Point Mixed-Delay Wavelet	32
Deterministic Reflectivity Function	34
Random Reflectivity Function	40
Mixed-Phase Air-Gun Wavelet	43
PARAMETERS	47
Length of the Initial Estimated Wavelet	47
Weights of the Initial Estimated Wavelet	47
Length of the Time Window	48
Offset Distance	48

	Page
Errors in the Velocity Function	48
STABILITY	51
CONCLUSIONS	59
REFERENCES	61

ACKNOWLEDGEMENTS

The author wishes to thank Dr. Fred Hilterman, thesis advisor, for all his encouragement and Dr. Milton Dobrin and Dr. John Butler for their valuable help.

The author would also like to thank Petroleo Brasileiro S. A. - Petrobras whose permission made it possible to complete this endeavor.

LIST OF FIGURES

Figure	Page
1. Common-Depth-Point technique of shooting	3
2. Synthetic CDP field record	7
3. Block diagram of pulse compression in frequency domain	12
4. Amplitude spectrum for source wavelet field traces	13
5. Application of the wavelet compression method for an isolated spike case	16
6. Application of the wavelet compression method for synthetic seismograms	17
7. Time domain application of the wavelet compression method. An isolated spike case	19
8. Time domain application of the wavelet compression method for synthetic seismogram . . .	20
9. Block diagram for converting r_0 to r_x and interpolating r_x to sample times t_x	25
10. Block diagram of the wavelet extraction solution	26
11. Wavelet and reflectivity extraction for a minimum-delay wavelet	29
12. Wavelet and reflectivity extraction for a maximum-delay wavelet	31
13. Wavelet and reflectivity extraction for a mixed-delay wavelet	33
14. Application of the wavelet extraction method to a synthetic deterministic function	36
15. Amplitude and phase spectra of the true wavelet used in the deterministic reflectivity model	37

Figure	Page
16. Output at various iterations of the wavelet extraction method	39
17. Application of the wavelet extraction method to a random function	41
18. Output at various iterations of the wavelet extraction process (random function)	42
19. Application of the wavelet extraction method to a mixed-phase air-gun wavelet	44
20. Amplitude and Phase spectra of the mixed-phase air-gun wavelet	45
21. Output at various steps of the wavelet extraction method (mixed-phase air-gun wavelet)	46
22. Application of the wavelet extraction method with a velocity function containing positive errors	50
23. Variation of the energy error at different offset distances	52
24. Application of the wavelet extraction method to an unstable model	54
25. Output at various iterations of the wavelet extraction method, (unstable model)	55
26. Amplitude and phase spectra of the true wavelet used in the unstable model	56
27. Amplitude and phase spectra of the estimated wavelet, one step before the instability	57
28. Output at various steps of the wavelet extraction method. Spike of the estimated wavelet at time zero	58

INTRODUCTION

One of the fundamental problems in exploration seismology is to obtain a seismic record which has both high resolution and high signal-to-noise ratio. If the seismic trace has a fair signal-to-noise ratio, then subsequent data processing can be applied to improve the resolution. This data processing technique is called deconvolution.

There are many forms of seismic deconvolution where each algorithm is based on assumptions about the seismic reflection model. Currently, one of the most popular seismic deconvolution algorithms has been described by Robinson and Treitel (1967). Their approach is based upon two theoretical assumptions. They are

- (1) the seismic wavelet is time-invariant and is minimum-phase, and
- (2) the primary events in the reflectivity function are randomly spaced in time and have random amplitudes.

However, there are many geologic environments where these assumptions are poor. Many geologic sequences have only a few stratigraphic features which are observed on seismic records as correlated events and thus the reflectivity function can be better described as a deterministic function, than as a random time series. Unfortunately, the exact amplitudes of this reflectivity function are not known so that the

deterministic model of the reflectivity functions is undefined.

An alternate method of describing the deterministic part of the reflectivity function is incorporated into a deconvolution process based upon two different theoretical assumptions. They are

- (1) the seismic wavelet is time-invariant and does not have any phase restrictions, and
- (2) the velocity function is known.

This study is concerned with the estimation of both the seismic wavelet and the reflectivity function using a known velocity function and seismic traces which have different source-receiver offsets.

STRUCTURE OF THE FIELD RECORD

In this study, the geologic model consists of horizontal layers and has multi-offset source-receiver locations that are symmetrically arranged about the reference point D_0 (See Figure 1). This is common depth point (CDP) recording. Further, the energy source produces a finite pulse of arbitrary shape which travels to the reflectors and back to the receivers without any distortion. The effects of transmission, wavefront divergence and changes in response due to different angle of incidence will be neglected.

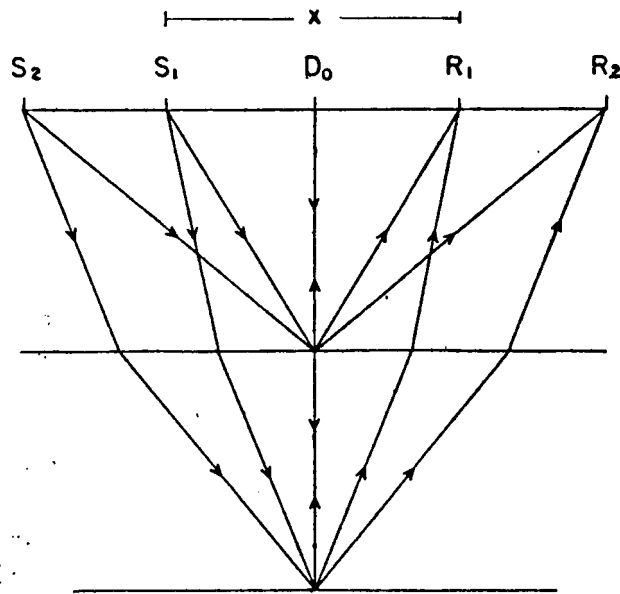


Figure 1. Common depth point technique of shooting. The subsurface points under D_0 are seismically sampled several times by the different source-receiver pairs which are symmetrically placed around D_0 .

According to Sengbush et al (1961), the zero-offset seismic trace is the convolution of the reflectivity function with the source wavelet, that is

$$s_o(t) = a(t) * r_o(t) \quad (1)$$

where: * = the convolutional operator,
 $s_o(t)$ = the seismic trace at zero offset,
 $r_o(t)$ = the reflectivity function at zero offset,
 and
 $a(t)$ = the seismic wavelet.

Nonzero-offset seismic traces are built up of the same sequence of primary events that went into the zero-offset trace. However, the reflectivity function will be compressed and delayed in time due to the normal move-out effect. An event which occurs at the two-way travel time of t_o on the zero-offset trace will occur at the time t_x on a trace which has a source-receiver separation of x . The straight raypath relationship for the NMO geometric factor is expressed as

$$t_{x,n}^2 = t_{o,n}^2 + x^2/v_{t_{o,n}}^2 \quad (2)$$

where: x = known offset distance,
 $t_{o,n}$ = arrival time of primary event n on trace at zero offset,
 $t_{x,n}$ = arrival time of primary event n on trace at x offset, and

$V_{t_{o,n}}^2$ = average velocity of the propagating wavelet
for a reflection from the nth interface.

Therefore, given a zero offset reflectivity function and a velocity function, the reflectivity function for a specified x , and t_o can be determined with the time transformation described in (2).

Figure 2c is an example of a synthetic 12-fold CDP field record derived from the geologic model represented by the interval velocity distribution and the seismic wavelet which are also shown in Figure 2. All twelve traces contain basically the same amount of information, that is, the primary events and the seismic wavelet. The difference between the traces is the density of information per unit time. In Figure 2c, any two traces are represented by the convolution of the time-invariant seismic wavelet with the corresponding reflectivity functions. For discrete data, these two traces can be represented as:

$$s_{o,i} = \sum_{j=0}^{\ell} a_j r_{o,i-j} \quad (3)$$

$$s_{x,i} = \sum_{j=0}^{\ell} a_j r_{x,i-j} \quad (4)$$

where: $s_{o,i} = s_o(i\Delta t) = s_o(t) \cdot \delta(t-i\Delta t)$,

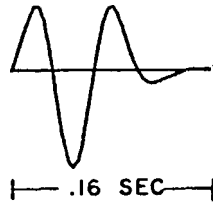
a = The seismic wavelet.

r_o = the reflectivity function at zero offset, and

r_x = the reflectivity function at offset x .

For ease of description, one of the traces has been selected at zero offset, however this is not a necessary requirement.

* * * * *



2a

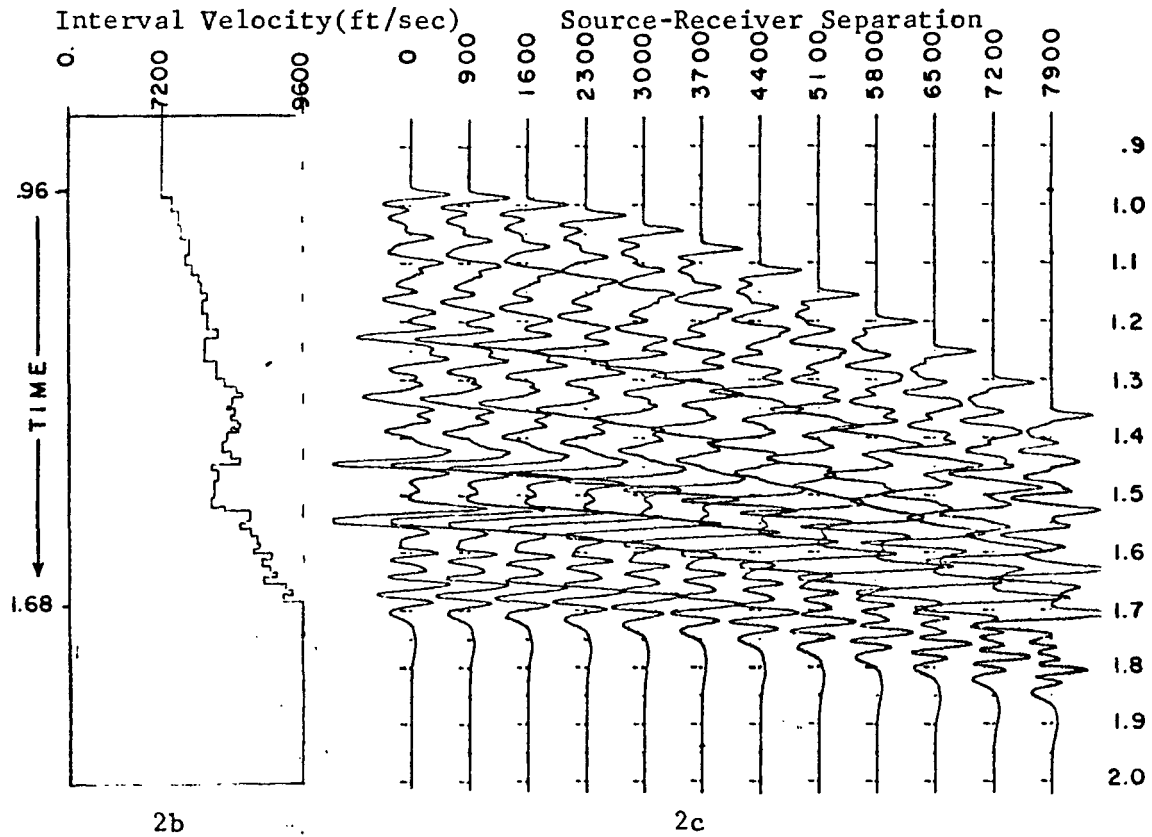


Figure 2. Synthetic CDP field gather. (a) source wavelet (b) interval velocity distribution of geologic model, and (c) synthetic seismogram generated by the convolution of the source wavelet with 12 reflectivity functions which were based on Figure 2b.

The reflectivity function r_x is a compressed and delayed expression of r_o . Energy which occurs on r_o at time t_o will occur with the same amplitude on r_x at the time t_x . The time t_o and t_x are related mathematically as $t_o = t_{xg}$ where the function g is described as:

$$g_i = \{V_i^2 \cdot (i\Delta t)^2 / [x^2 + V_i^2 \cdot (i\Delta t)^2]\}^{1/2} \quad (5)$$

The function g like the velocity functions is time dependent.

For very shallow reflectors (5) is not valid. This is because the two-way path to shallow events for the propagating seismic wavelet is almost the same as the direct path, and the character of the reflection is lost. To avoid this problem, a time-window on s_o and its corresponding compressed time window on s_x were selected. Also, both windows were shifted to zero time. So in this study (3) and (4) will refer to time-shifted windows.

The solution of (3) and (4) for the seismic wavelet and the reflectivity function is not simple, mainly because the function g is time variant. If g were constant, the time relationship between r_o and r_x would be linear and the seismic wavelet could be estimated easily within a constant phase and scalar factor. This method is a simple application of the time scaling property of the Fourier Transform.

The function g is usually not a multiple of the sample rate, therefore the relationship $t_o = t_{xg}$ yields

times other than the discrete sampled times and thus a two-point interpolation scheme is used in this study to convert r_0 into r_x .

* * * * *

WAVELET COMPRESSION TECHNIQUE

Frequency Domain

The normal moveout correction which is widely applied in CDP data processing consists of stretching the trace with x -offset in order to represent a zero-offset trace. In contrast, the opposite method will be done for pulse compression. That is, the trace with zero-offset will be compressed to simulate a trace with x -offset.

The inverse application of NMO and its relationship to pulse compression is shown by the block diagram in Figure 3. The input parameters are the velocity function, the offset and both seismic traces. The output of the second step is an estimate of the seismic trace at x -offset. This estimated trace is viewed as having the same reflectivity function as the field trace at this offset but the seismic wavelet is compressed by g which is given in (5). Moreover, as g is a function of t_0 , this compression will be different at each lag of the window. So, the application of the function g on s_0 has the same effect as an application of a time-varying filter which compresses the seismic wavelet. The time-varying compressed wavelet has undesirable high frequency components which are not present in the field trace at offset x (See Figure 4). In order that these erroneous frequency components were not propagated in the recursive

algorithm, a zero-phase bandpass filter was applied to the estimated trace, $\hat{S}_x(w)$, as shown in step 4 of Figure 3.

Now, by dividing in the frequency domain the data-processed compressed trace by the field trace, a digital filter which compresses the wavelet is estimated, and this filter is applied to the zero-offset field trace. This is shown by steps 5 and 6 in Figure 3.

* * * * *

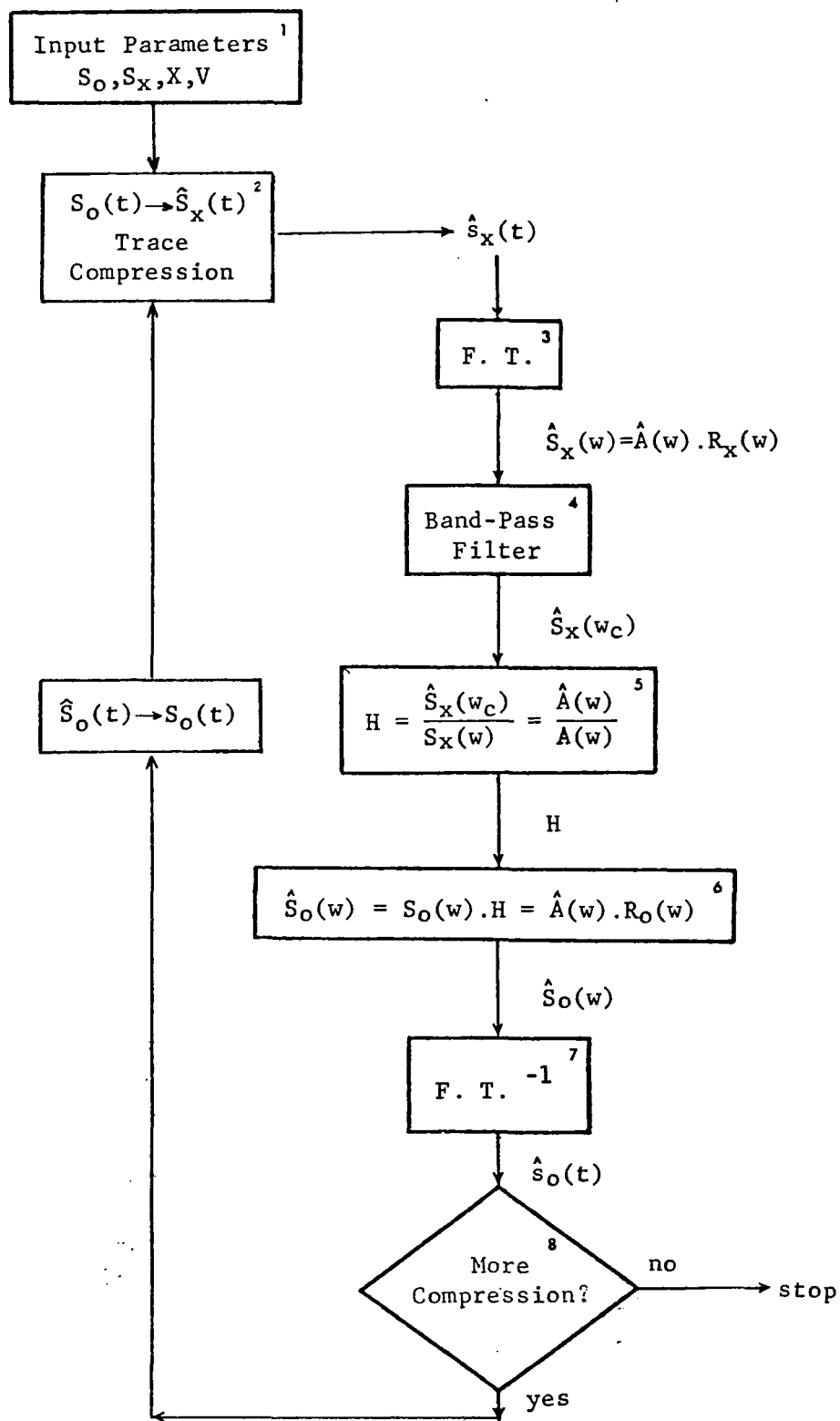


Figure 3. Block diagram illustrating pulse compression in the frequency domain.

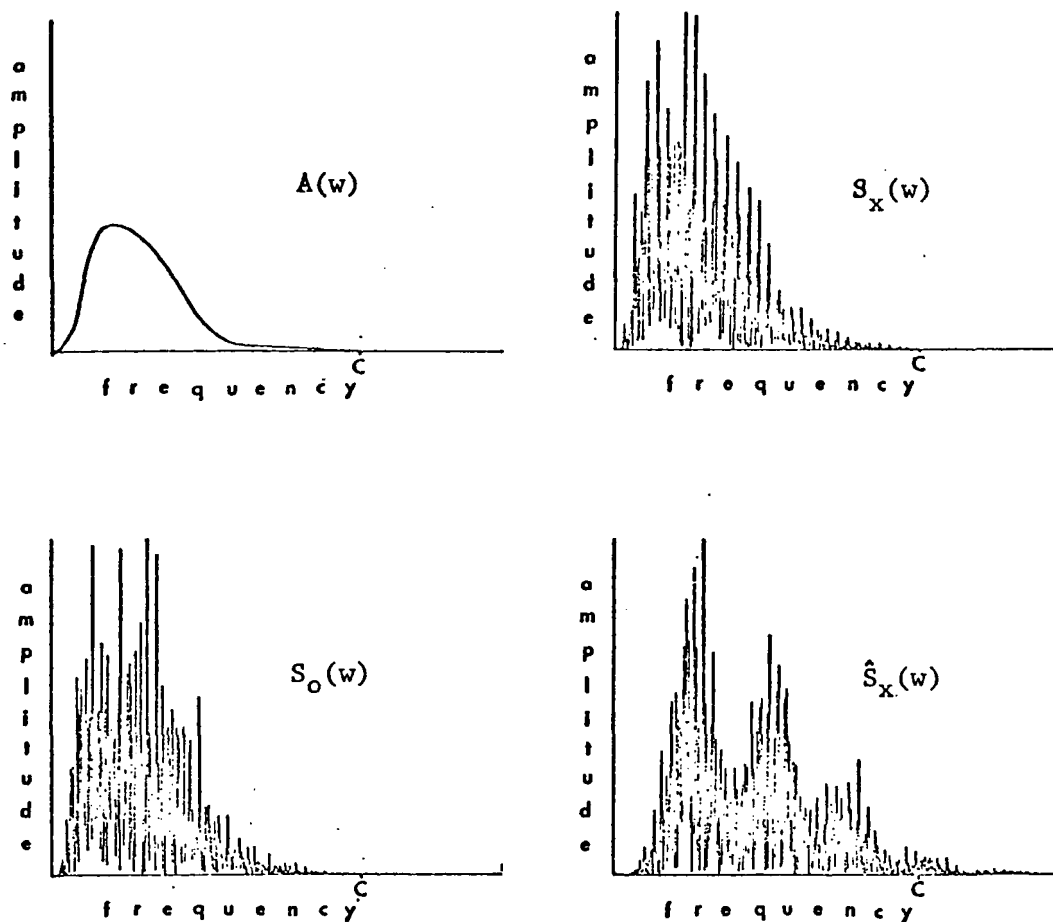


Figure 4. Diagrammatic view of amplitude spectra for source wavelet, field traces s_o , s_x and estimated field trace \hat{s}_x .

The inverse Fourier Transform of the resulting trace yields the trace at zero offset with the true wavelet replaced by the estimated compressed wavelet (output of step 7).

This process is repeated many times to hopefully improve the resolution of the seismic trace.

The estimated wavelet has a broad frequency spectrum but because $S_x(w)$ does not have appreciable energy at high frequencies there is a possibility of generating high frequency noise by the division performed in step 5. This is why the bandpass filter is applied in step 4. Another reason for applying the bandpass filter is that compressing the wavelet is similar to resampling a time series and the original time series cannot have frequencies above the new Nyquist frequency. For pulse compression, this upper frequency component can be approximated by

$$(f_N) \hat{s}_x = \frac{\Delta t - (\Delta t_1 - \Delta t_2)}{\Delta t} \cdot f_N$$

where: Δt_1 = NMO correction for the first sample in the

time window of s_0 which is used to predict s_x ,

Δt_2 = NMO correction for the second sample,

Δt = sample rate of s_0 time series,

f_N = Nyquist frequency of $s_0 = \frac{1}{2} \Delta t$, and

$(f_N) \hat{s}_x$ = upper frequency components in s_0 allowable
if s_x is predicted from s_0 .

For the cases presented in this study a 1Hz-180Hz bandpass was applied because the upper allowable frequency

component was approximately 187 Hz as computed from the equation for $(f_N)\hat{s}_x$.

On the other hand, the filter removes important frequencies of the time varying wavelet. Without these high frequencies the wavelet will not converge to a spike but only to some bandlimited approximation. Too high a cut-off frequency will generate noise which increases with the number of iterations in the predicted trace. This effect will be seen in the following examples.

Example 1: An Isolated Spike case.

Figure 5 shows an example where the reflectivity function consists of an isolated spike (trace at left) at a time of .96 sec. The velocity was set at 7200 ft/sec and the offset at 3700 ft. Trace zero corresponds to zero offset and in this trace it is possible to see the shape of the original wavelet. Traces 1,2,3,.....,10 correspond to iterations 1,2,3,.....10 of the process. The window length was .25 sec and a 1Hz-180Hz bandpass filter was applied.

The hyperbolic rate of compression that is evident in Figure 5 is related to the normal moveout, from which the method is derived. In this example the compression gives significant results without introducing too much noise. This is an ideal pulse compression.

* * * * *

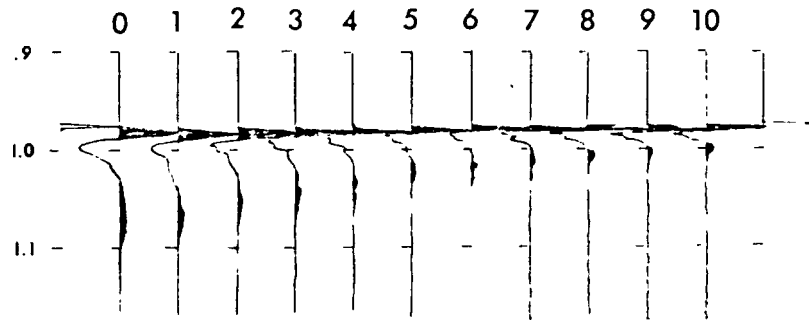


Figure 5. Application of the wavelet compression method in a model consisting of a reflectivity function which is a simple spike. The filter was calculated in the frequency domain.

Example 2: Synthetic Seismogram.

A more realistic example is shown in Figure 6. The first trace (left) corresponds to the reflectivity function which is repeated at the right for scaling purposes. The offset was 3700 ft and the velocity function was applied with an average error of -1%. A 1Hz-180Hz bandpass filter was applied at each iteration. Trace zero is the zero offset trace of Figure 2c and corresponds to a 0.5 sec window taken from 1.25 sec to 1.75 sec. Traces 1,2,3,.....,7 are the output of iteration 1,2,..7.

In Figure 6a as well as in Figure 5, the effect of time-varying compression is quite evident. The last .1 sec of the window gate represents the original tail of the seismic wavelet and its distortion is due to the high frequency component left in the system and this noise increases with the number of iterations. This high frequency distortion is present through the window gate of the synthetic trace, but

it is partially masked by the convolutional overlap. The compression does increase the resolution of the synthetic trace, as is evident at 1.38 sec and at 1.60 sec.

In step 3 of Figure 3 any discrepancy in the estimation of the reflectivity function is related to the estimated wavelet. This was designed so that small errors in the velocity function affect the performance of the compression itself, without generating undesirable and unpredictable time shifts in the original data. In fact, Figure 6a shows that the events do not shift as the number of iterations increase, even though an intentional error in the velocity function was present.

Figure 6b illustrates the same example without application of the bandpass filter. The propagation of high frequency noise in the system is clearly shown.

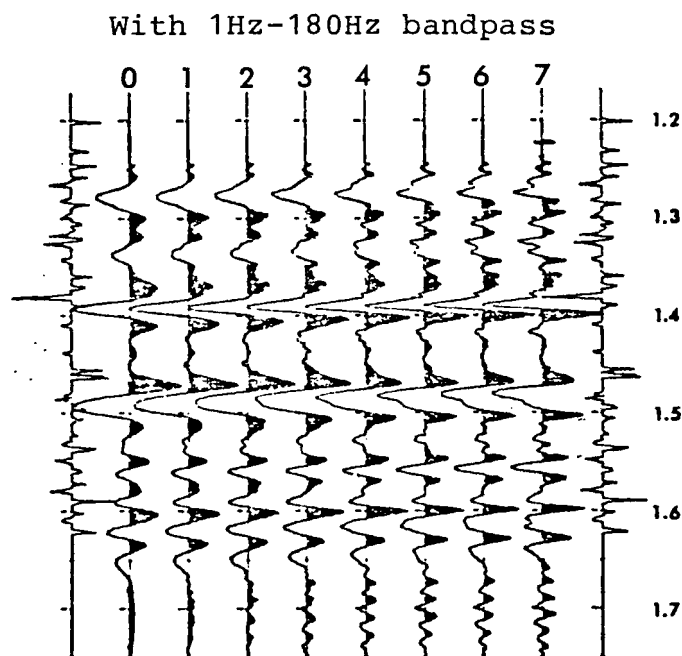


Figure 6 a. Frequency domain application of the wavelet compression method.

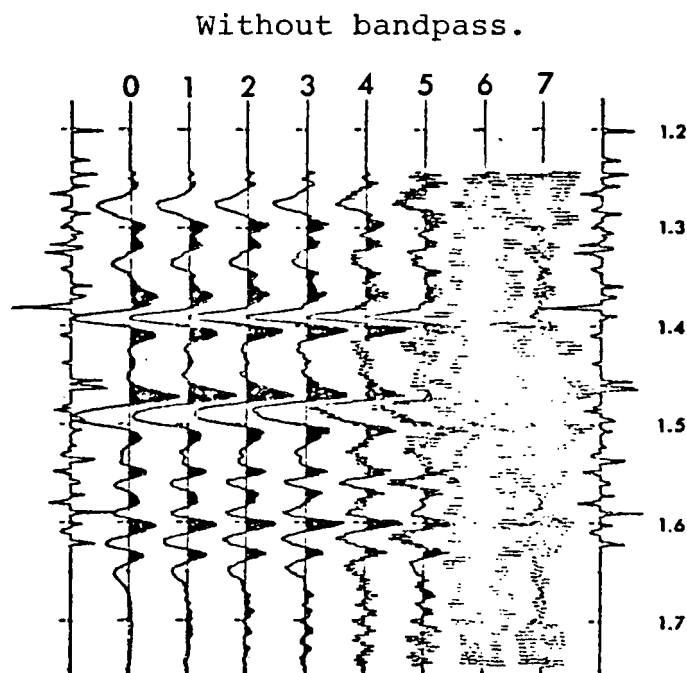


Figure 6b. Frequency domain application of the wavelet compression method.

Time Domain

Pulse compression can be done in the time domain by using an alternate method for finding the inverse operator H in step 5 of Figure 3. Even though this method failed, the ideas described here were the origin of the wavelet extraction method described in the next part of this study.

In Figure 3, after step 2, the first estimate of the trace at x -offset is given. Now instead of going to the frequency domain, a least square shaping filter is designed so that when it is convolved with the field trace at offset x it yields the estimated trace. That is

$$s_x(t) * h(t) = \hat{s}_x(t) \quad (6)$$

where: $h(t)$ = the shaping filter.

The filter design and implementation follows the general theory of shaping filters described by Treitel and Robinson (1966).

Convolving this filter, $h(t)$, with the trace at zero offset will generate the next compressed version of the trace, and by repeating this process an increase in resolution is attempted.

Example 1: An Isolated Spike case.

When the reflectivity function is an isolated spike, the results are shown in Figure 7. The effect of compression is evident, but the error in the velocity function time-shifts the reflection and this time-shift increases with the number of iterations.

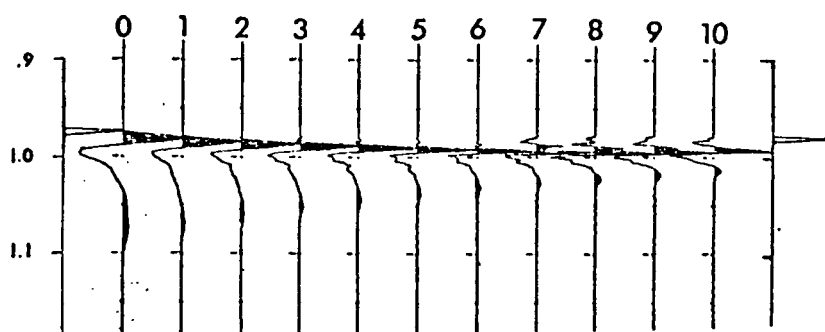


Figure 7. Time domain application of the wavelet compression method.

* * * * *

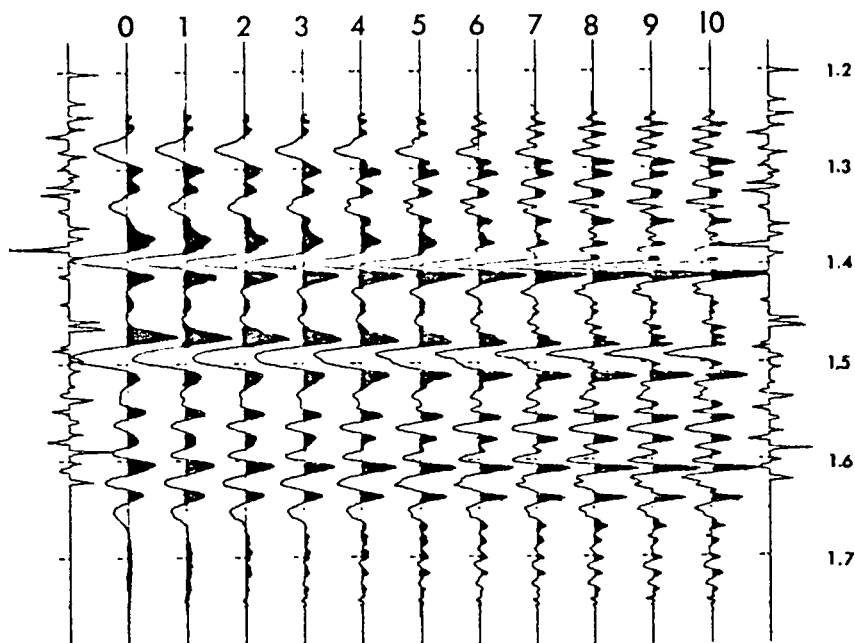


Figure 8. Time domain application of the wavelet compression method. Note the shifts that are introduced on the individual events.

Example 2: Synthetic Seismogram.

Figure 8 shows the results that are obtained when the shaping filter is applied to the same set of information that generated Figure 6. A 1Hz-180Hz bandpass filter was also applied at each step. It is evident that the compression is good. The noise introduced by the filter is generally the same in the lower part of the window but is higher in the beginning of the window where there is more compression. An undesirable feature shown in Figure 7 is the time shifts that the filter introduces on each event. The small (-1)% error due to the velocity function increases the time shift at each iteration. As a mean of compensation for this time error, a non-causal least-square shaping filter could have been designed. This however would then require a search algorithm

to determine the time shifts. This process was not tried because the wavelet extraction technique which is described in the next section bypassed this possible problem.

A least-square solution was attempted for one direction (from zero offset to x offset) but it was not applied for the reverse direction. When using the shaping filter approach for both directions, it is possible to recover not only the wavelet but also the reflectivity function. This idea is discussed in the next step of this study.

where the α -matrix is called the Normal Move-Out Transform-mation matrix (NMOT). This matrix is computed from the velocity function and the offset distance as

$$\alpha_{ij} = \beta_{ij} + \gamma_{ij} \quad (9)$$

where:

$$\begin{array}{lll} \beta_{ij} = h_j - i + 1 & 0 < \beta_{ij} \leq 1 & \beta_{ij} = 0 \\ \gamma_{ij} = i - h_j + 1 \text{ only if} & \text{otherwise} & \\ \beta_{i1} = 0 & 0 < \gamma_{ij} \leq 1 & \gamma_{ij} = 0 \end{array}$$

and

$$h_j = (j + b - 1)/g(j + b - 1) - b/g_b + 1 \quad (\text{See Figure 9})$$

* * * * *

For two windows in two different seismic traces, where the zero offset is selected as one of the input traces for convenience, the matrix notation of convolution yields for $s_o(t)$ and $s_x(t)$

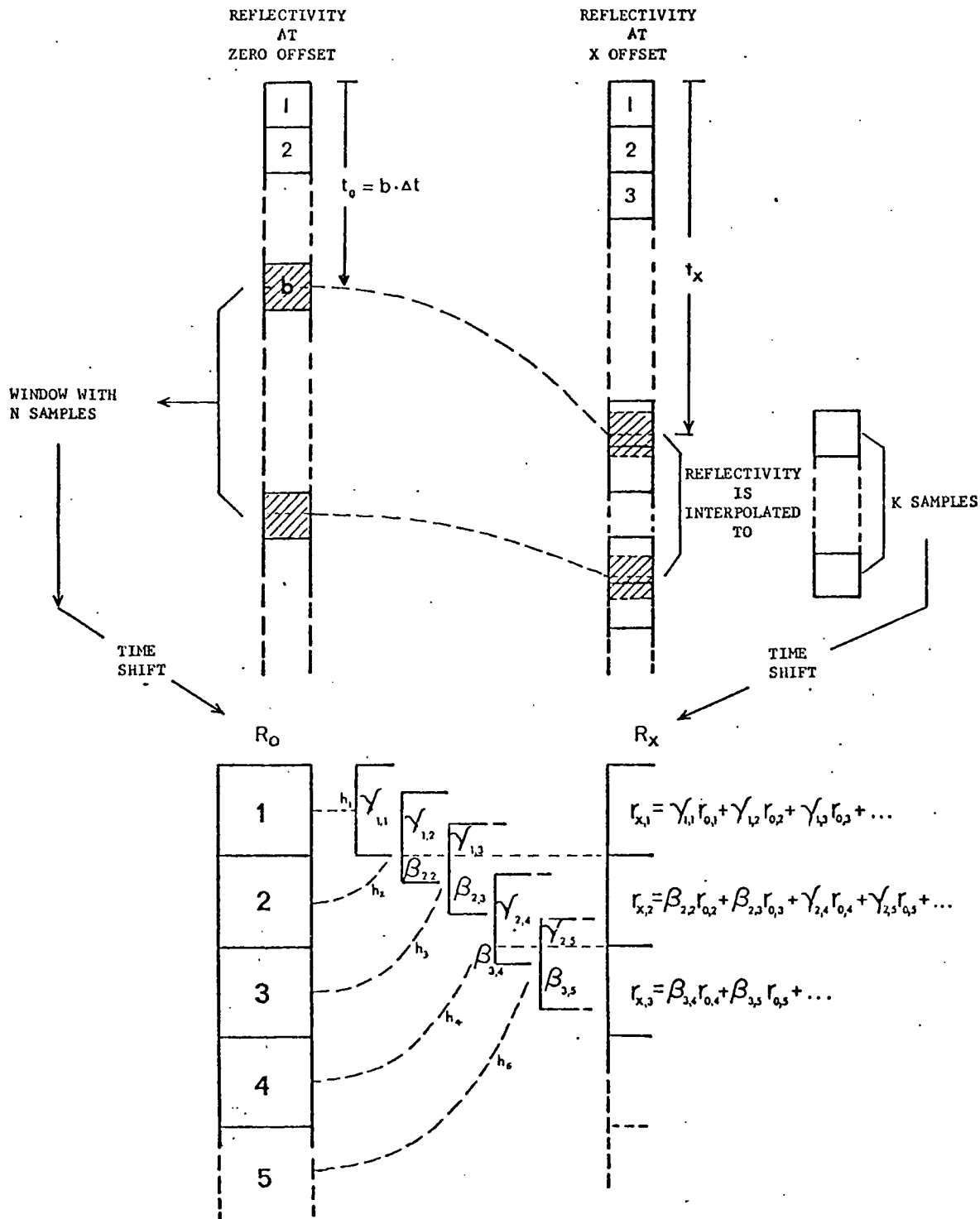


Figure 9. Block diagram for converting r_0 to r_x and interpolating r_x to sample times.

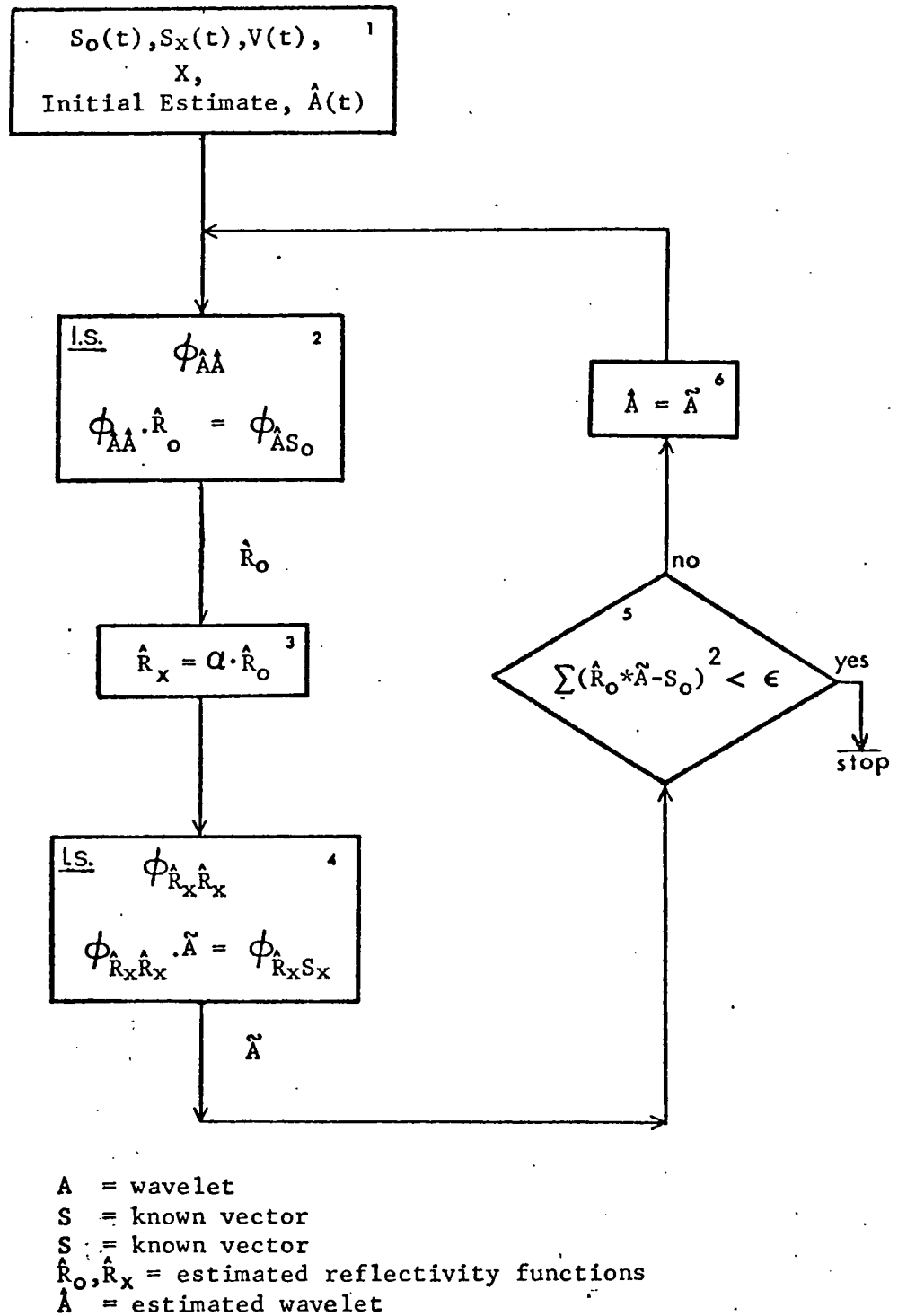


Figure 10. Block diagram illustrating the wavelet extraction solution of equations (10) and (12).

In step 2 and 4 the familiar least square shaping filter algorithm is applied. However, the meaning of the shaping filter is slightly changed for each step. For step 2, an estimate of R_0 is computed and for step 4 an estimate of the desired wavelet A is computed.

Hopefully, the wavelet estimate, \hat{A} , convolved with the reflectivity estimate, \hat{R}_0 , reproduces the seismic trace at zero offset. With this estimation of the wavelet the next iteration can be started. When the original wavelet is recovered the error criteria as defined in step 5 of Figure 10 is zero. Also, the successive iterations will give the same output. In other words, the system stabilizes when the exact wavelet is obtained.

The following simple models illustrate the wavelet extraction technique described in Figure 10.

Two Point Minimum Delay Wavelet.

Input data: $S_0 = (.2, .94, -.7, .12, 0., 0., 0.)$

$S_x = (.74, -.162, -.018, 0., 0.)$

$\hat{A} = (1., 0., 0.)$

$n = 7$

$k = 5$

$L = 3$

Computed NMOT matrix	$\left \begin{array}{cccccccc} 1.0 & 0.6 & .15 & 0. & 0. & 0. & 0. & 0. \\ .0 & .4 & .85 & .7 & .2 & 0. & 0. & 0. \\ .0 & .0 & .0 & .3 & .8 & .6 & .1 & 0. \\ .0 & .0 & .0 & .0 & .0 & .4 & .9 & 0. \\ .0 & .0 & .0 & .0 & .0 & .0 & .0 & .0 \end{array} \right $
from a given velocity	

Desired output: $A = (1., -.3)$

$R_0 = (.2, 1., -.4)$

Figure 11 shows various iterations of the system. A comparison of the output for iteration 18 with the desired output demonstrates that the solutions for the seismic wavelet and for the reflectivity function are excellent.

* * * * *

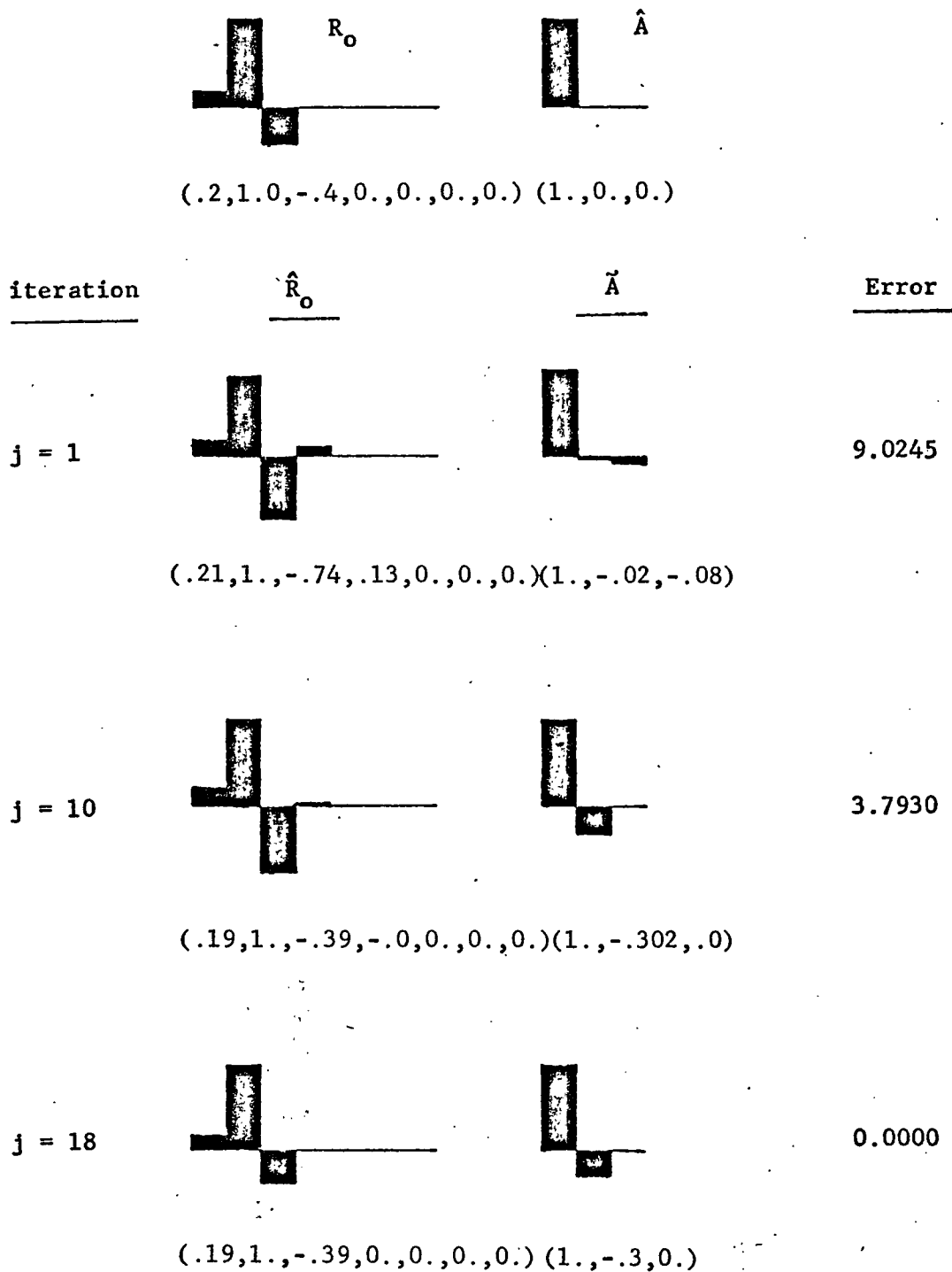


Figure 11. Wavelet and reflectivity extraction for a minimum-delay wavelet.

Two Point Maximum Delay Wavelet.

Input data: $S_o = (0.04, .4, .92, -.4, 0., 0., 0.)$

$S_x = (.148, .752, .06, 0., 0.)$

$\hat{A} = (1., 0., 0.)$

$n = 7$

$k = 5$

$L = 3$

NMOT = same as in preceding example.

Desired output: $A = (.2, 1.)$

$R_o = (.2, 1., -.4)$

Figure 12 shows various iterations of the system. After 37 iterations an excellent solution was obtained. If the first estimate had been better, the final solution would have been accomplished with less iterations, as was the case in the Minimum Delay example.

* * * * *

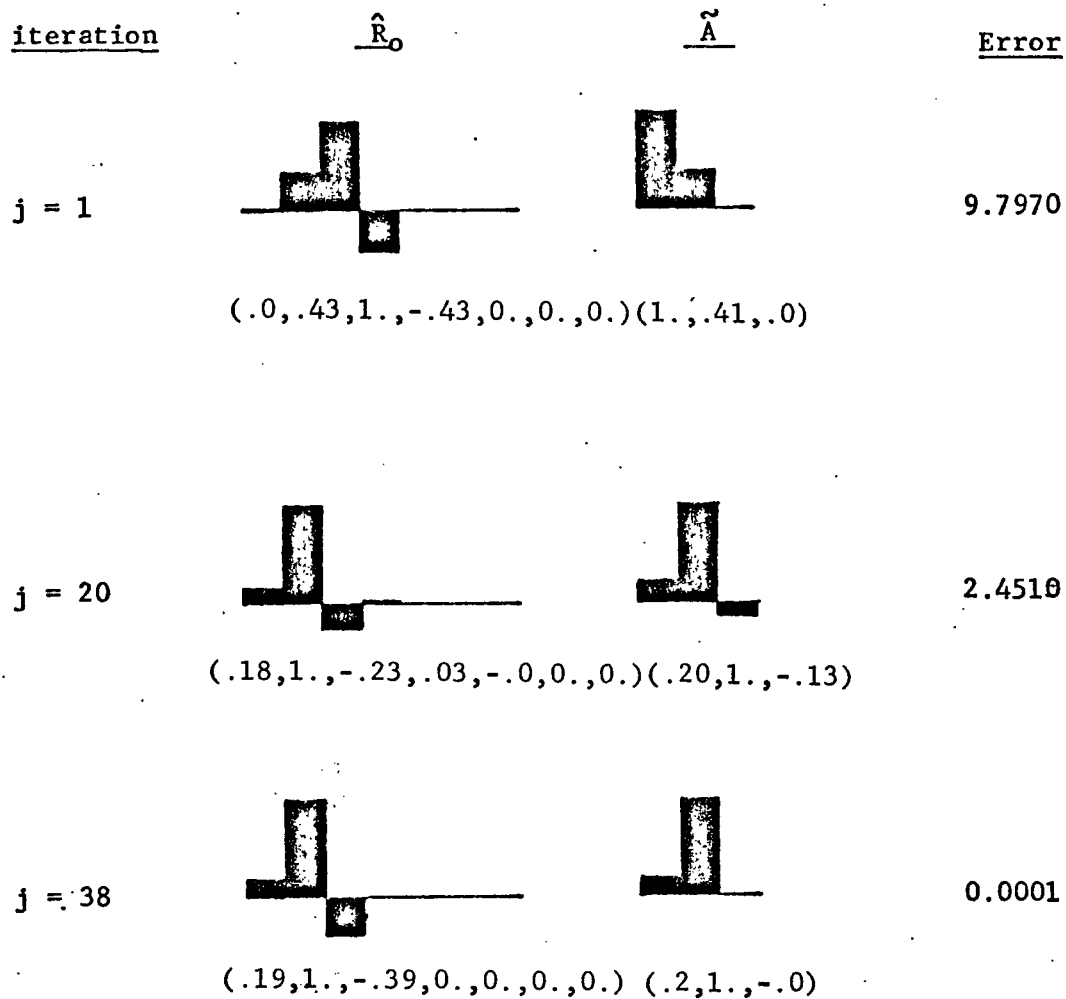
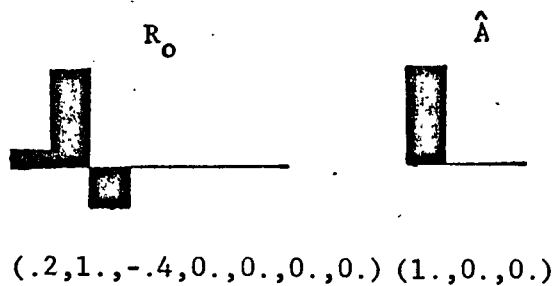


Figure 12. Wavelet and reflectivity extraction for a maximum-delay wavelet.

Three Point Mixed-Delay Wavelet

Input data: $S_O = (.02, .3, .98, -.29, .06, .01, 0., 0.)$

$S_X = (.074, .753, .207, .043, .003, 0.)$

$\hat{A} = (1., 0., 0., 0.)$

$n = 8$

$k = 6$

$L = 4$

Computed NMOT	1.0	.6	.15	0.	0.	0.	0.	0.
from a given velocity	.0	.4	.85	.7	.2	0.	0.	0.
	.0	.0	.0	.3	.8	.6	0.	0.
	.0	.0	.0	.0	.0	.4	.1	0.
	.0	.0	.0	.0	.0	.0	.9	.5
	.0	.0	.0	.0	.0	.0	.0	.5

Desired Output: $A = (.1, 1., .1)$

$R_O = (.2, 1., -.4, .1)$

Figure 13 shows that 17 iterations yields the desired output.

* * * * *

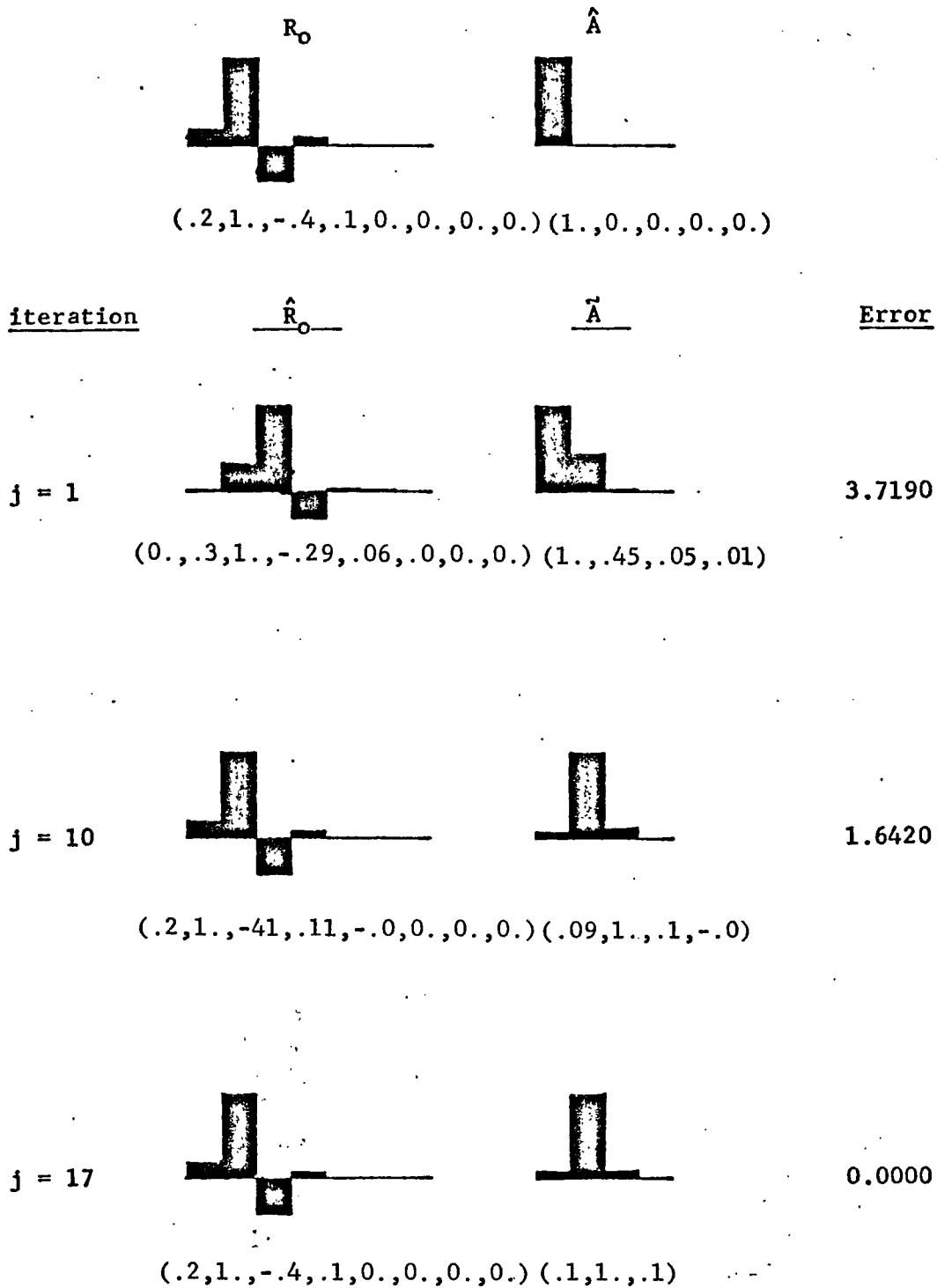


Figure 13. Wavelet and reflectivity extraction for a mixed-delay wavelet.

These three examples illustrate how the system is independent of the shape of the reflectivity function and the shape of the wavelet. In fact, no assumptions were made about the shape of the seismic functions and no restrictions were imposed during the mathematical development of the method.

Deterministic Reflectivity Function.

A better feeling about the performance of the method is given by the example illustrated in Figure 14. The reflectivity function (14b) consists of 6 isolated spikes with different amplitudes which were distributed in a window of .38 sec. The true wavelet consists of a 32-point minimum-phase wavelet whose amplitude and phase spectra are shown in Figure 15. At zero-offset the convolution of this wavelet with the reflectivity function yields the synthetic seismic trace whose shifted window is shown on Figure 14b. With the velocity function shown in Figure 14a and assuming an offset distance of 2000 ft., the corresponding compressed version of the reflectivity function was computed and convolved with the true wavelet to yield the synthetic seismic trace s_x .

The offset, the velocity function and both synthetic traces were loaded into the system described in Figure 10.

The conditions to stop the iterations were either an error less than 0.01 or 100 iterations whichever happened first.

The initial estimate of the wavelet was a spike

followed by 39 zeros and the result after 100 iterations was the estimated wavelet shown in Figure 14c.

* * * * *

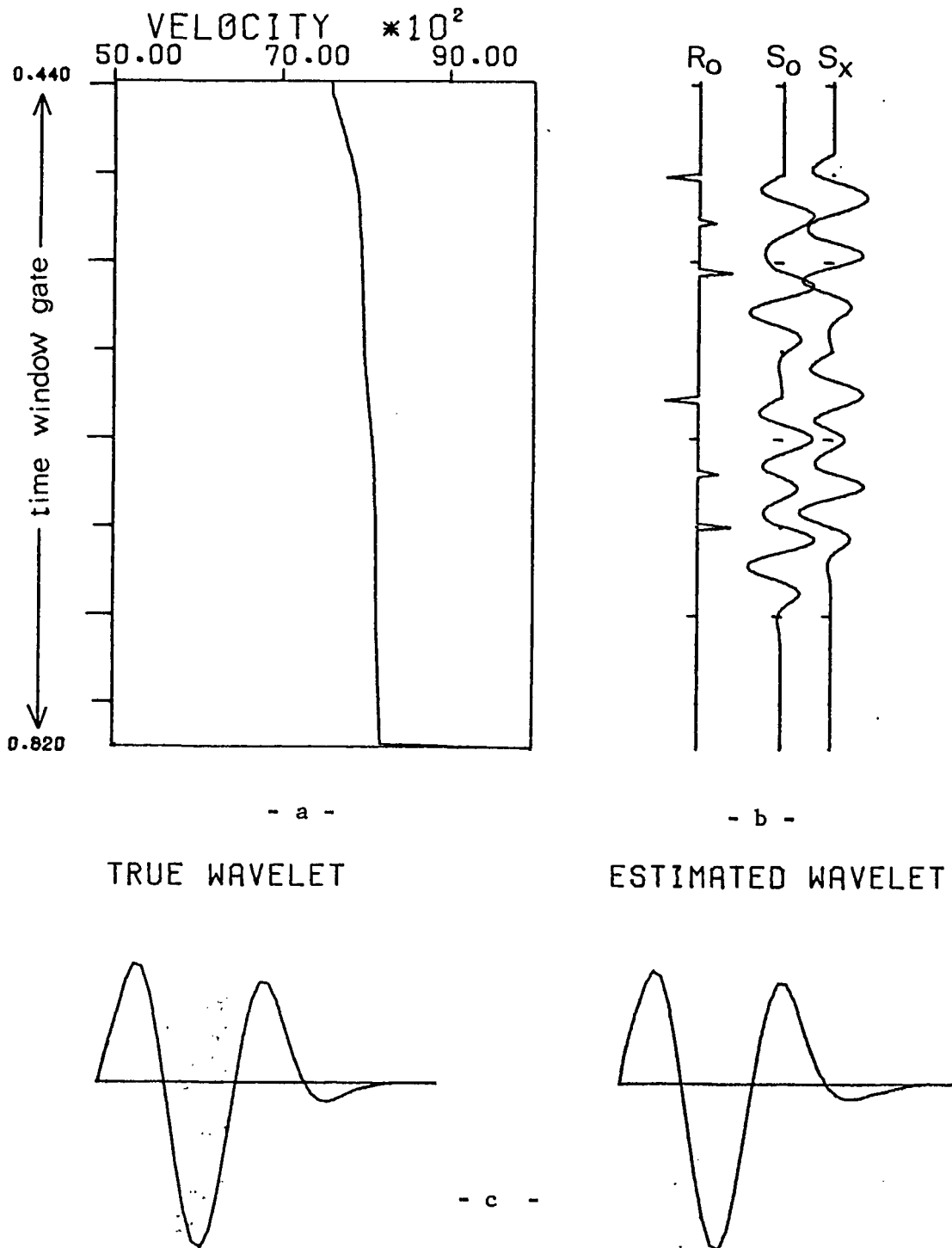
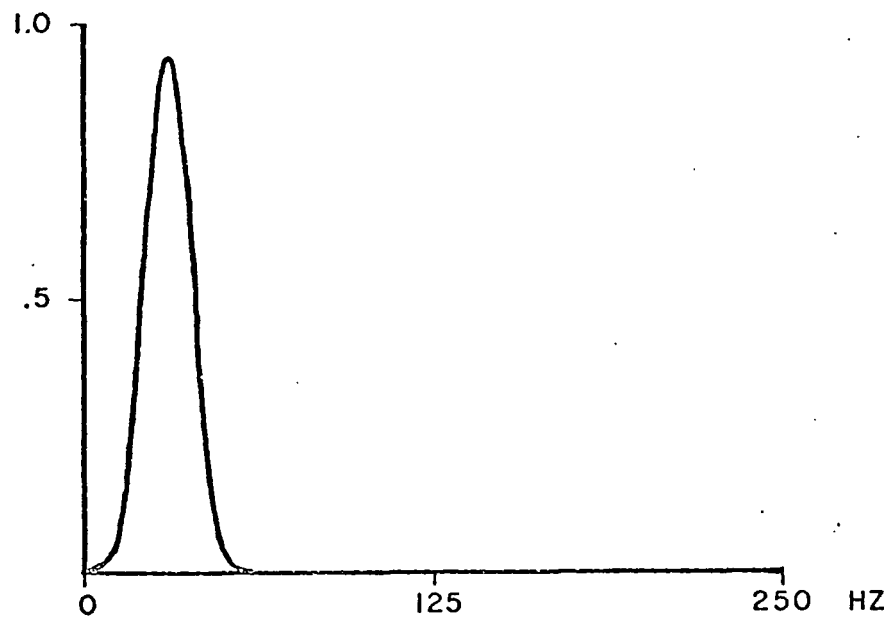
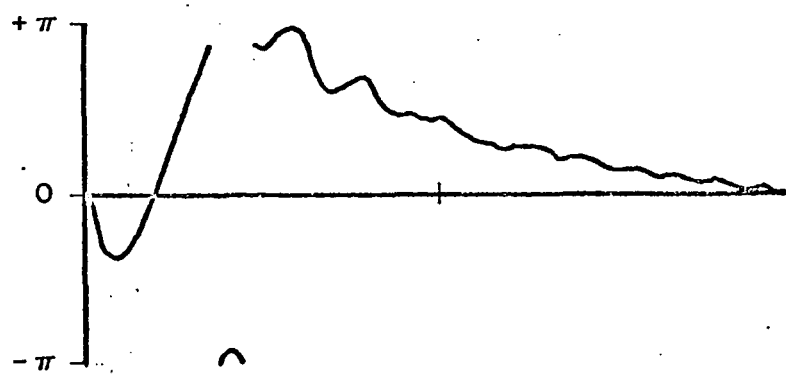


Figure 14. Application of the wavelet extraction method to a synthetic deterministic function. (a) The average velocity function, (b) The original reflectivity function at zero offset, the corresponding seismic trace, and trace at 2000 ft. (c) True wavelet and estimated wavelet after 100 iterations.



- Amplitude -



- Phase -

Figure 15. Amplitude and Phase spectra of the true wavelet used in the deterministic reflectivity model.

Figure 16 shows different steps of the process. The initial wavelet ($j=0$) yields the first estimate of the reflectivity function ($j=1$) which is the seismic trace itself. The estimated reflectivity function of the last iteration is a reasonable approximation of the actual one.

* * * * *

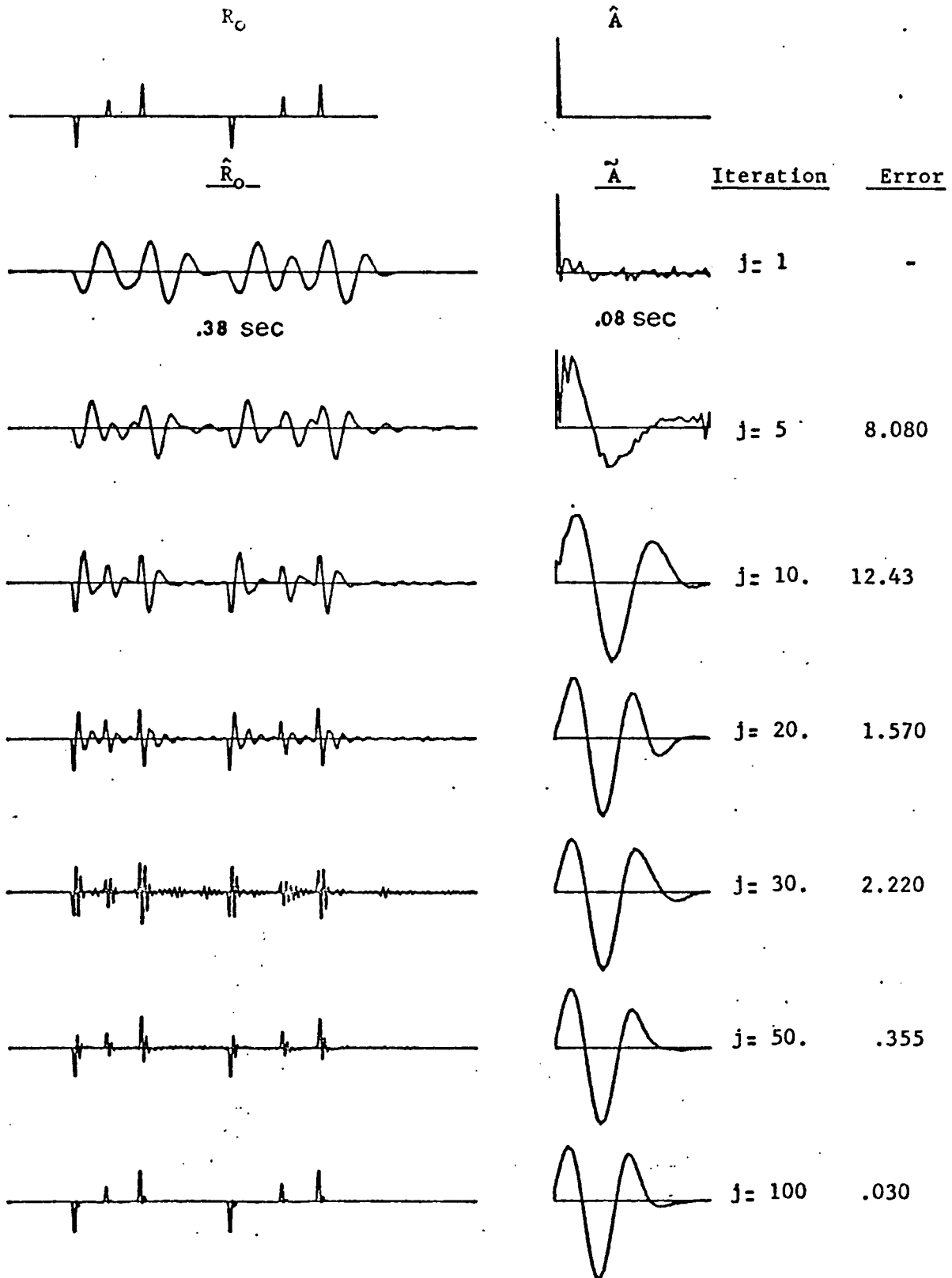


Figure 16. Outputs at various iterations of the wavelet extraction method.

Random Reflectivity Function

Figure 17 is another example of the method, where the zero offset reflectivity function is random. The true seismic wavelet and the velocity function are the same as in the preceding example. A time window of .38 sec and an offset distance of 3500 ft. were used. The two resulting synthetic seismic traces have their shifted windows shown in Figure 17b. The estimated seismic wavelet after 100 iterations is shown on Figure 17c.

Figure 18 shows various steps of the process. After 100 iterations the estimated reflectivity function was recovered. However, the changes in the wavelet estimates is due to instability and this will be discussed later.

* * * * *

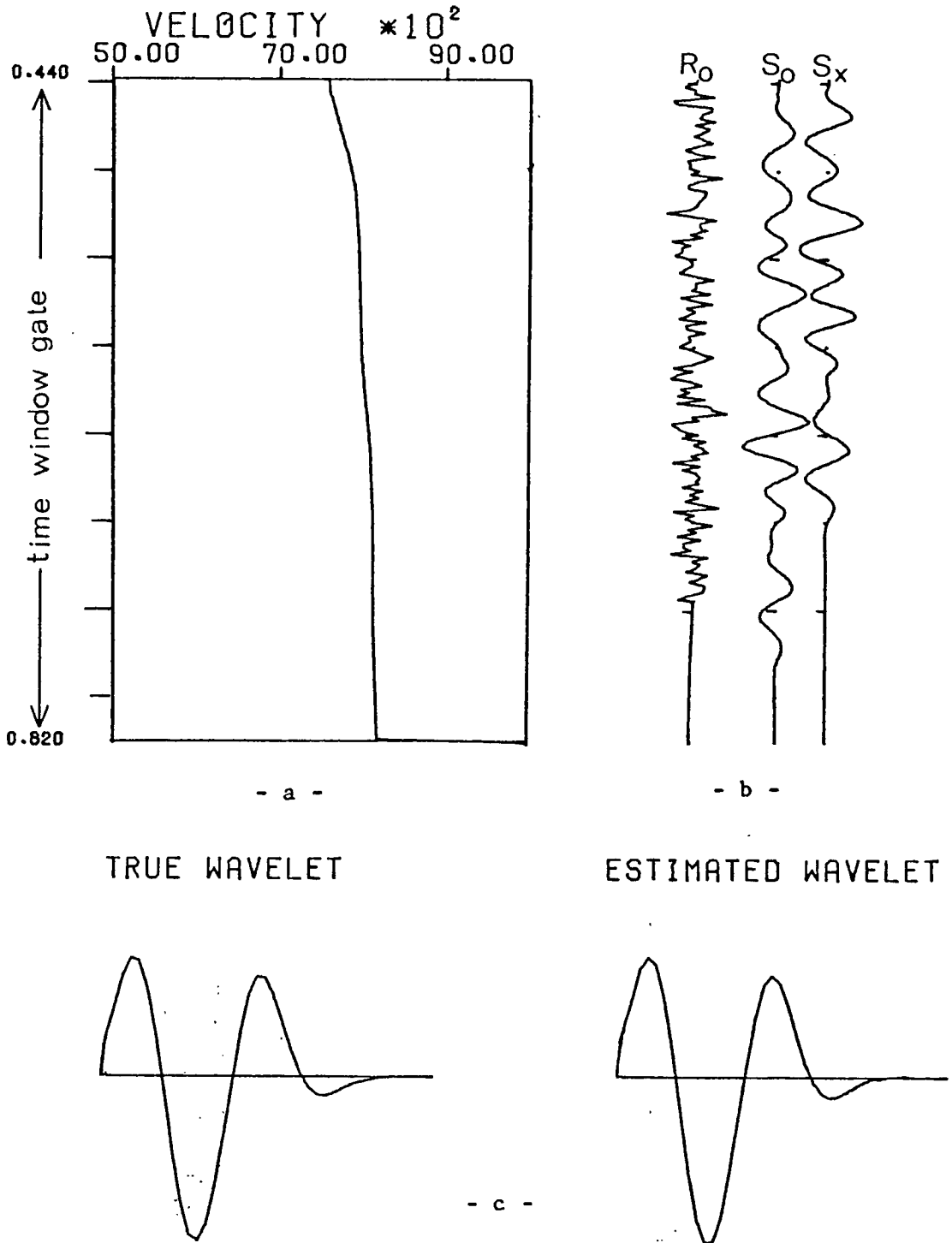


Figure 17. Application of the wavelet extraction method to a random function. (a) The average velocity function. (b) The original reflectivity function, the seismic trace at zero offset and at 3500 ft. (c) True and estimated wavelet after 100 iterations.

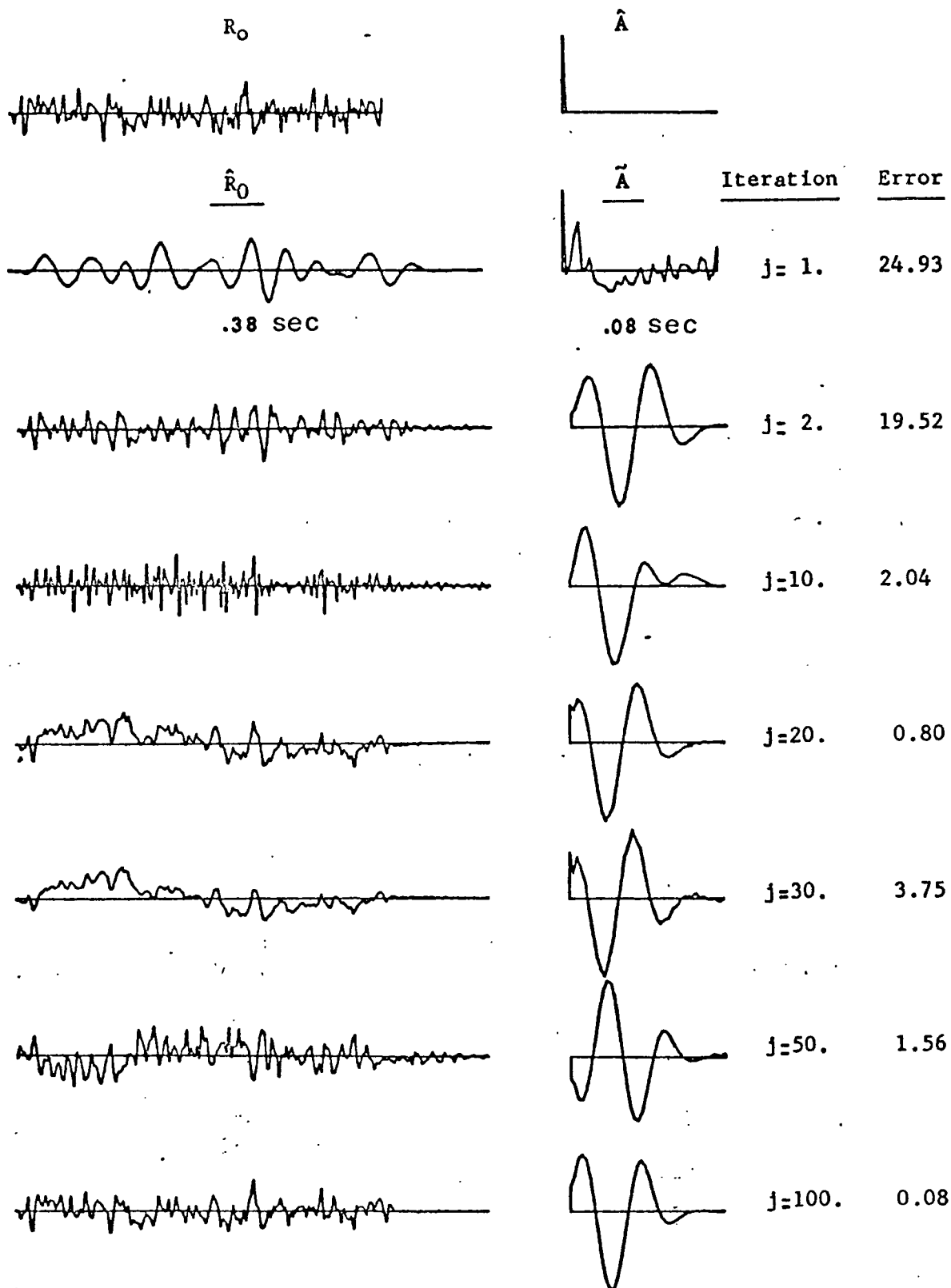


Figure 18. Outputs at various iterations of the wavelet extraction process. Note the similarity of the estimated reflectivity function at $j=100$ with the actual reflectivity function.

Mixed Phase Air-Gun Wavelet

Figure 19b shows a model with a mixed-phase air-gun wavelet. Its amplitude and phase spectra are shown in Figure 20. The time window was taken from .440 sec to .854 sec with the velocity function as shown in Figure 19a. The offset distance was 5000 ft. The estimated wavelet after 17 iterations is shown on Figure 19c.

Figure 21 shows the output at various iterations. The recovered reflectivity function reproduces all the details of the actual reflectivity function.

* * * * *

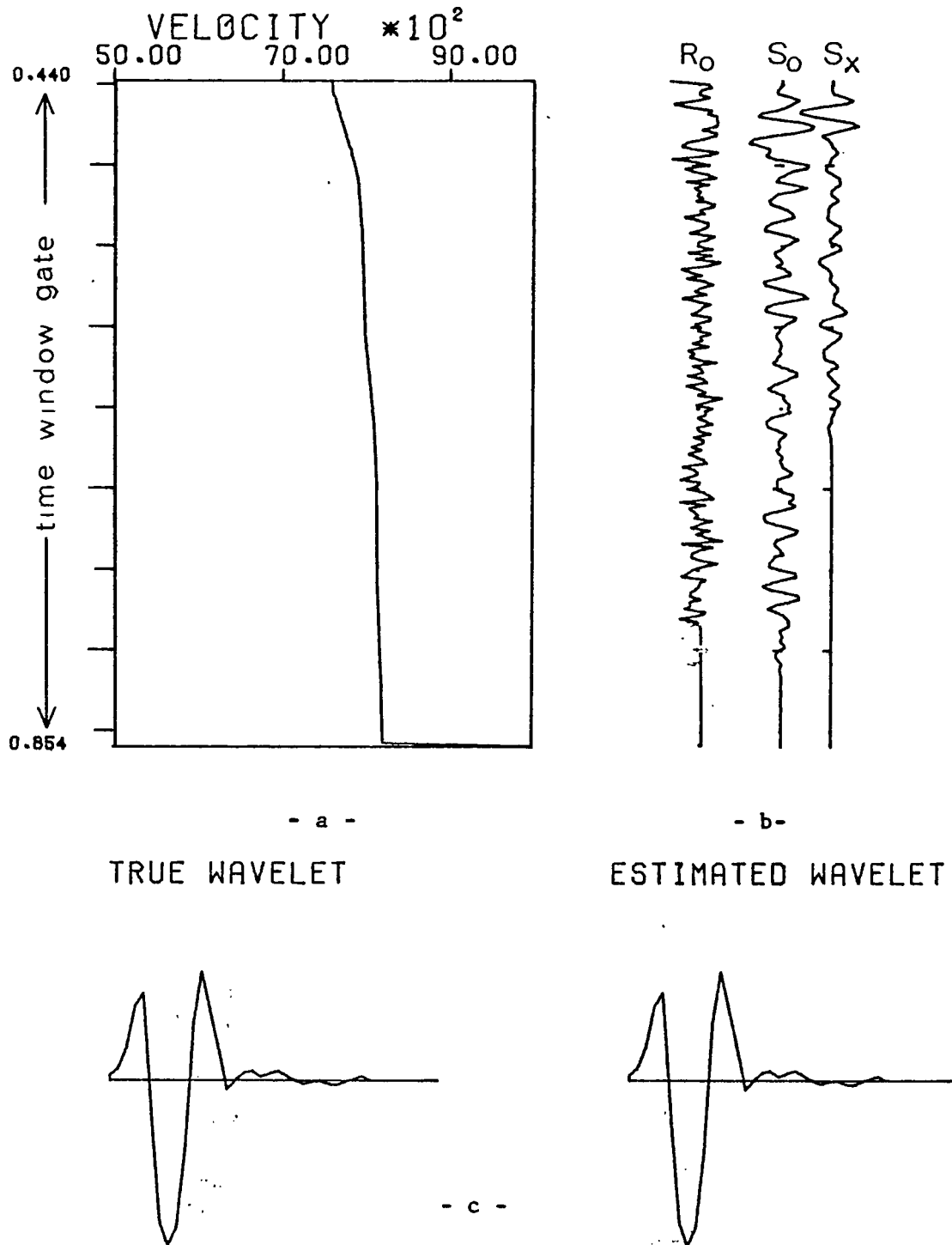
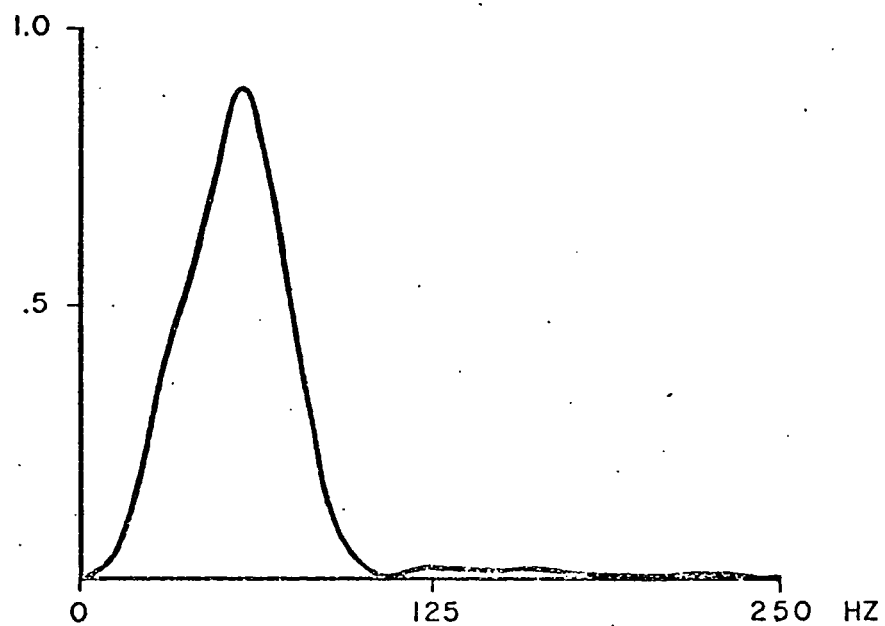
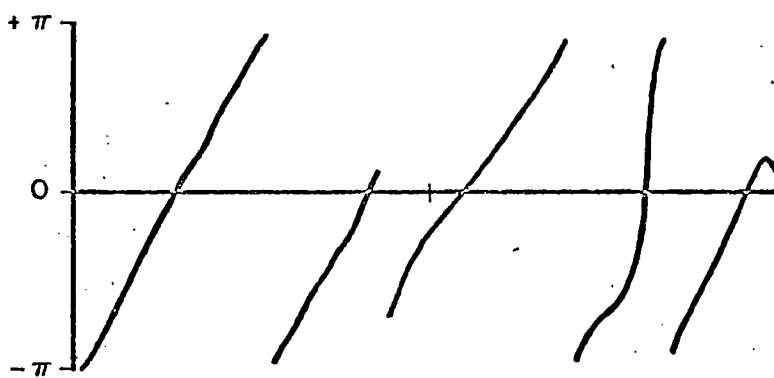


Figure 19. Application of the wavelet extraction method to a mixed-phase air-gun wavelet. (a) The average velocity function. (b) The actual reflectivity function, the seismic trace at zero offset and at 5000 ft. (c) The true wavelet and the estimated wavelet after 17 iterations.



Amplitude



Phase

Figure 20. Amplitude and Phase spectra of the mixed-phase air-gun wavelet.

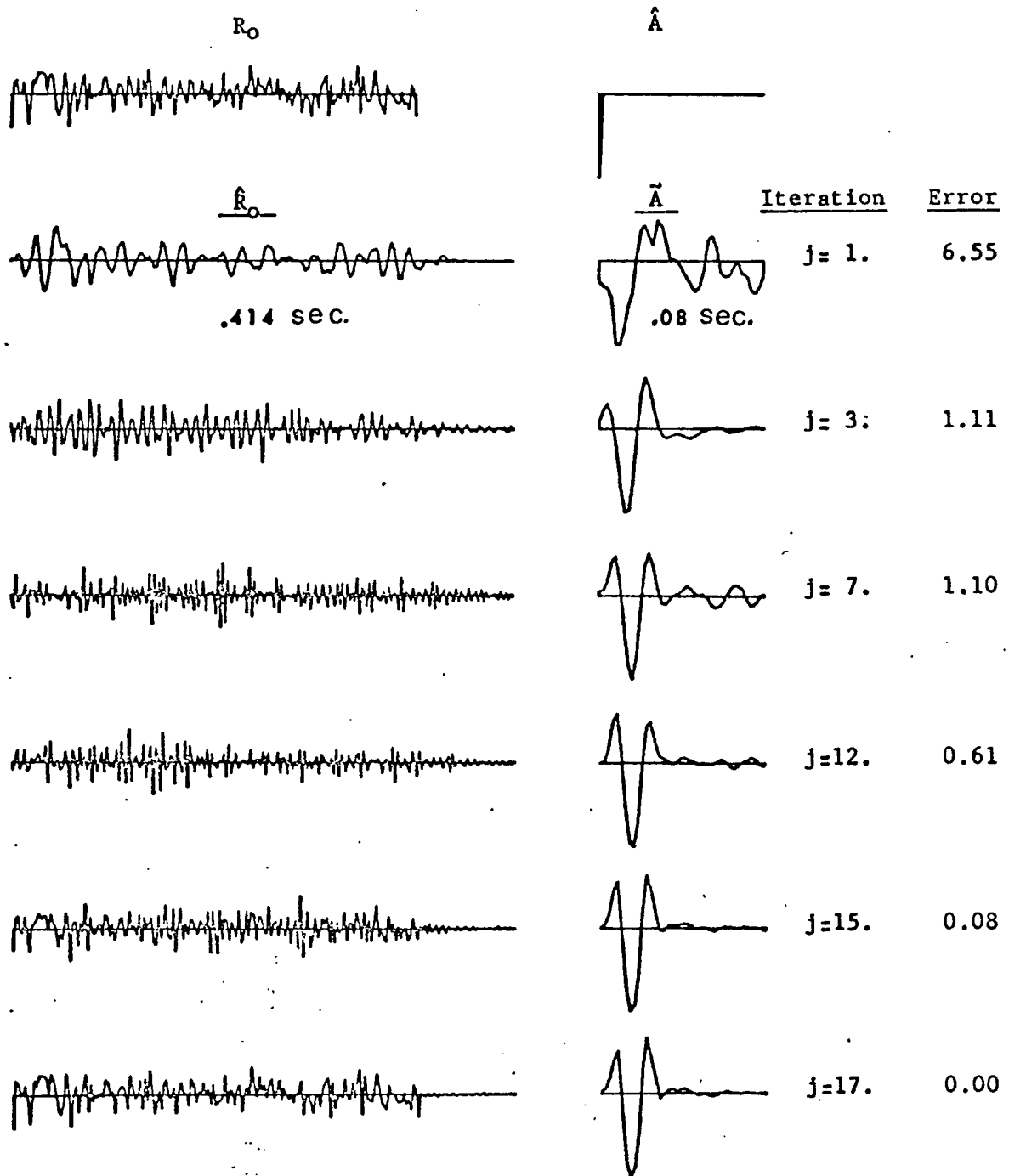


Figure 21. Output at various steps of the wavelet extraction method. The process stops in 17 iterations when the error criterion was satisfied.

PARAMETERS

The parameters which govern the rate of convergence of the system are:

- the length of the initial estimated wavelet,
- the weights of the initial estimated wavelet,
- the length of the time window gate,
- the offset distance, and
- the errors in the velocity function.

Length of the Initial Estimated Wavelet

The estimation of the seismic wavelet for each iteration is performed by step 4 in Figure 10 which is the output of a shaping filter. In general, the longer the filter, the faster the convergence of the system. The minimum length of the initial estimated wavelet must be at least the same length of the true wavelet, otherwise the system will not be able to converge. Normally, a reasonable length will have to be defined from the seismic section by the geophysicist.

Weights of the Initial Estimated Wavelet

On the examples studied, it is easy to see that if an initial wavelet is estimated with a shape similar to the output after n iterations, then n iterations of the process will be saved. A good initial estimate would be a simple spike which contains all frequencies. Attempting to approximate the desired output may generate problems in cases where the initial estimate does not contain all frequencies component which are in the seismic traces. On some estimated wavelets the polarity was inverted, but the performance of

the extraction system did not change.

It is always possible to depict a reasonable shape for the initial estimate from the seismic section. In marine work, the deep water bottom reflections may give a good approximation.

Length of the time window gate.

One important feature that is not discussed in this study is the end effects which always appear when working with time windows. A suitable truncation must be performed to avoid these problems and the window length must be chosen as a function of the truncation operator. Also, the window must contain several good reflectors that are compressed in order to improve the performance of the shaping filters.

Offset Distance.

Normally, the larger the offset distance, the smaller the NMOT matrix will be thus increasing the rate of convergence of the system. However, the offset distance can not assume values which generate NMOT matrices which are smaller than the seismic wavelet ($k < L$ in equation 12). When the NMOT matrix approximates the identity matrix, which occurs at small offsets, no compression is performed and the method is not applicable. In the next section the stability of the system for different offsets will be discussed.

Errors in the velocity function.

The higher the average velocity error, the slower

will be the wavelet convergence. Eventually, no convergence at all will be obtained. The errors will generate a distorted output. It is preferable to have a positive error in the velocity function rather than a negative error. This is related to the fact that the lags of the crosscorrelation functions are computed only for positive values in order to avoid a maximum coherence search.

Figure 22 shows an example of a velocity function containing positive errors. Figure 22a is the true and the overestimated velocity functions which are applied in the process. Figure 22b shows the reflectivity function, the seismic trace at zero offset s_0 and the seismic trace at 4000 ft. offset. Figure 22c shows the true and the estimated wavelet after 50 iterations. It is necessary to point out that the process was not stable. The stability of the system is discussed in the sequence of this study.

* * * * *

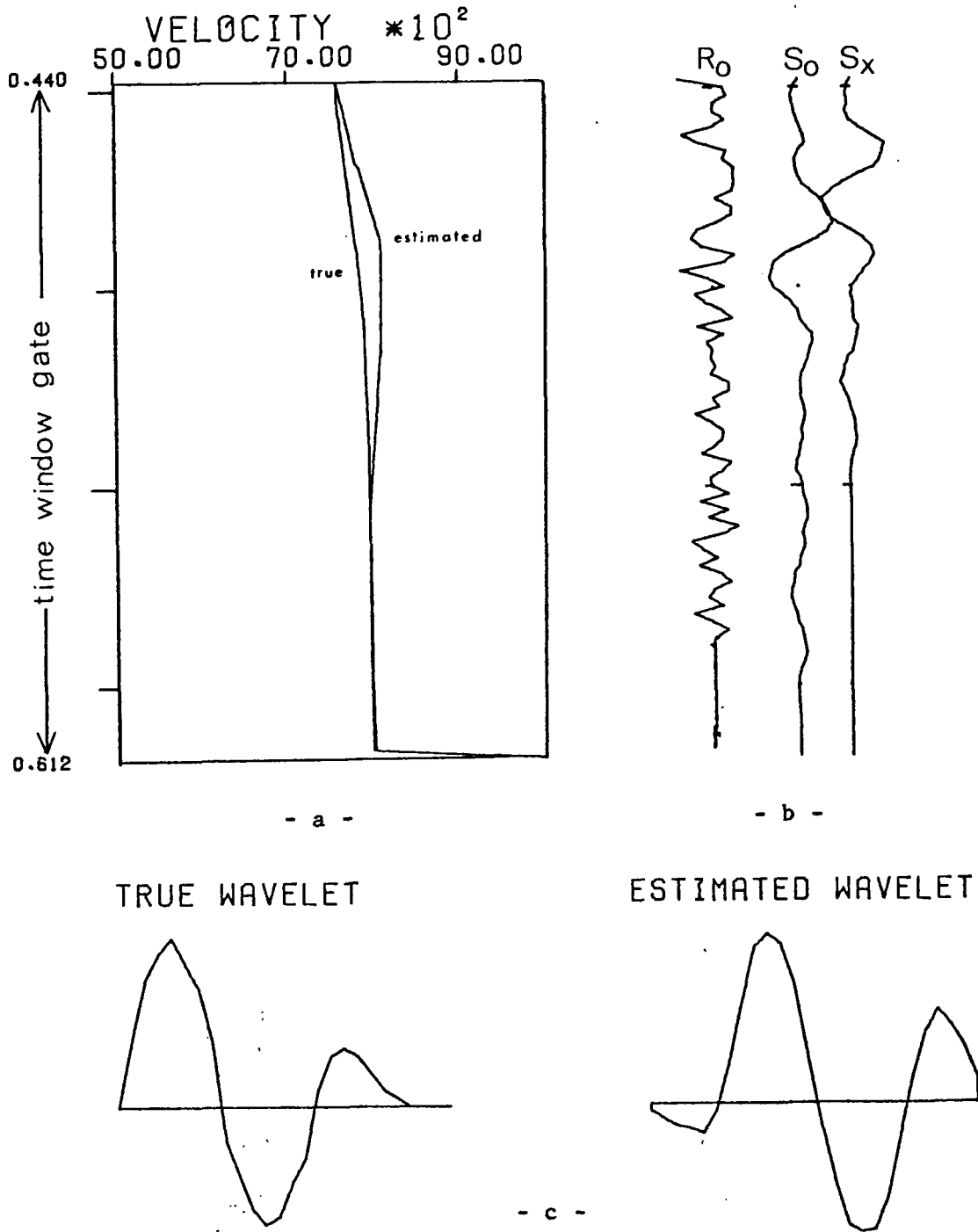


Figure 22. Application of the wavelet extraction method with a velocity function containing positive errors. (a) The true and overestimated velocity functions. (b) The actual reflectivity function, the seismic trace at zero and at 4000 ft. (c) The true and estimated wavelet after 50 iterations.

STABILITY

Stability, which is related to zero points in the power spectrum of the estimated wavelet is the major problem encountered in this study. Solutions of this problem had been attempted without success.

The example of the minimum-phase wavelet shown in Figure 14 was intentionally used to demonstrate some characteristics of an unstable model. It is expected for the energy error to decrease uniformly to zero, and this was not the case. In order to better visualize the problem, the same example was run using different offsets. Figure 23 shows the variation of the energy error with number of iterations for various offset distances.

This stability problem is the same as that described in the wavelet compression technique. In particular, step 2 in Figure 10 computes an estimated wavelet which is bounded in the frequency domain or contains values in the amplitude spectrum which are close to zero. As unstable deconvolution is a zero division in the frequency domain, the time domain equivalent is a nonpositive definite autocorrelation matrix. An attempt to stabilize the system was made by adding white noise to the autocorrelation matrix. This did stabilize the system but did not allow the system to converge to a minimum error criteria.

* * * * *

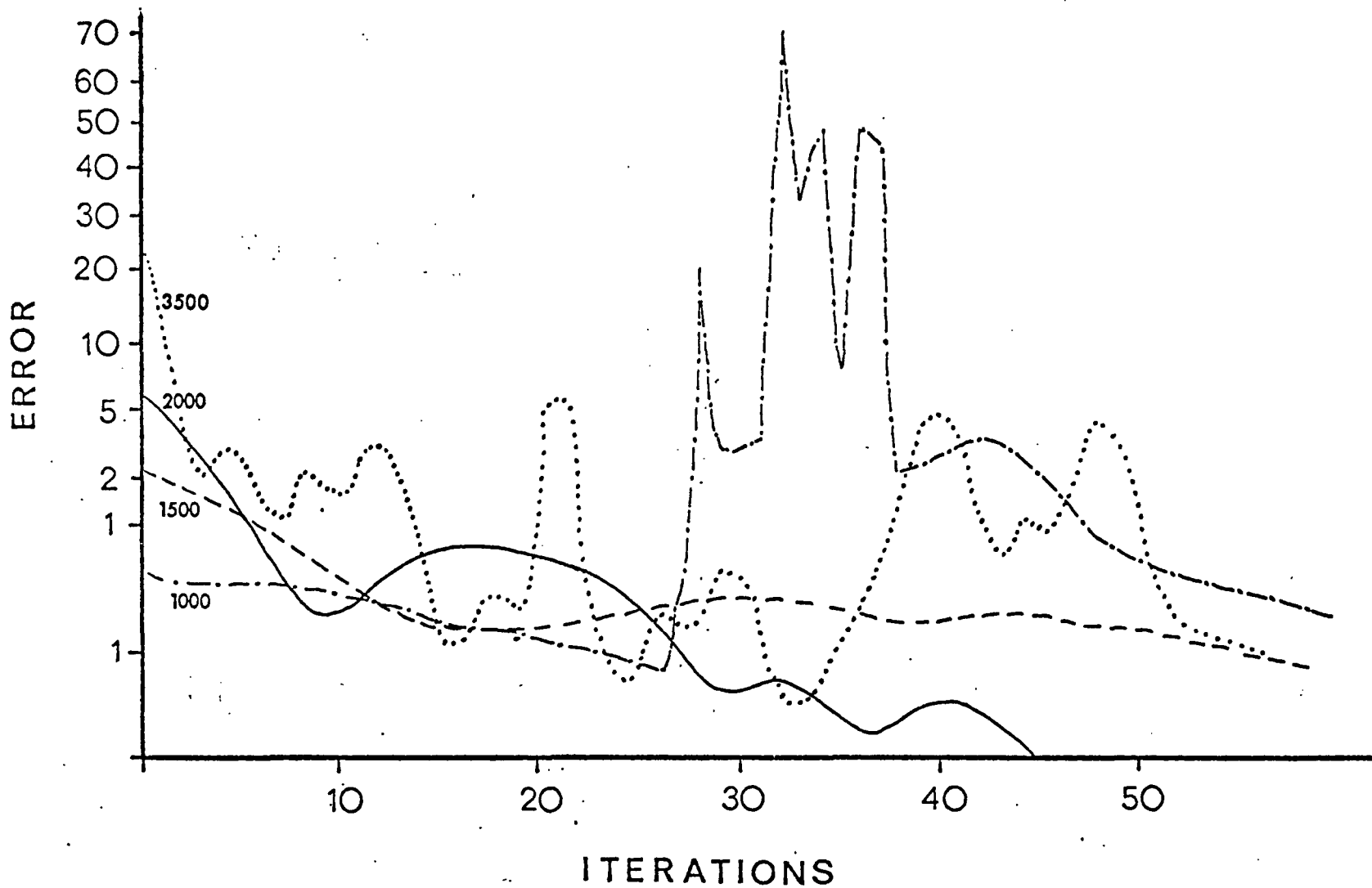


Figure 23. Variation of the energy error at different offset distances.

Figures 24 and 25 illustrate a system that could not overcome a wavelet estimate that had a near zero frequency point. When a 0.001% increment was added to the zero lag autocorrelation, the system stabilizes with the wavelet shown of the 13th iteration. However, this is not close to the true wavelet.

Figure 26 is the power spectrum of the true wavelet. The amplitudes of frequencies higher than 60 Hz are insignificant, but different from zero as shown on the detailed scale. Figure 27 is the power spectrum of the estimated wavelet one iteration before the instability. Even with a detailed scale, amplitudes of frequencies higher than 60 Hz are zero, or at least less than 10^{-6} .

This analysis suggests future work is necessary for those situations where the spectrum of the source wavelet decays rapidly such as would be the case in Vibroseis data.

The same example was tested with the initial estimate of the wavelet with a spike in the first sample. The system behaves in the same way, as expected, and the result one step before the instability is shown in Figure 28. With addition of white noise it stabilizes in this different shape.

* * * * *

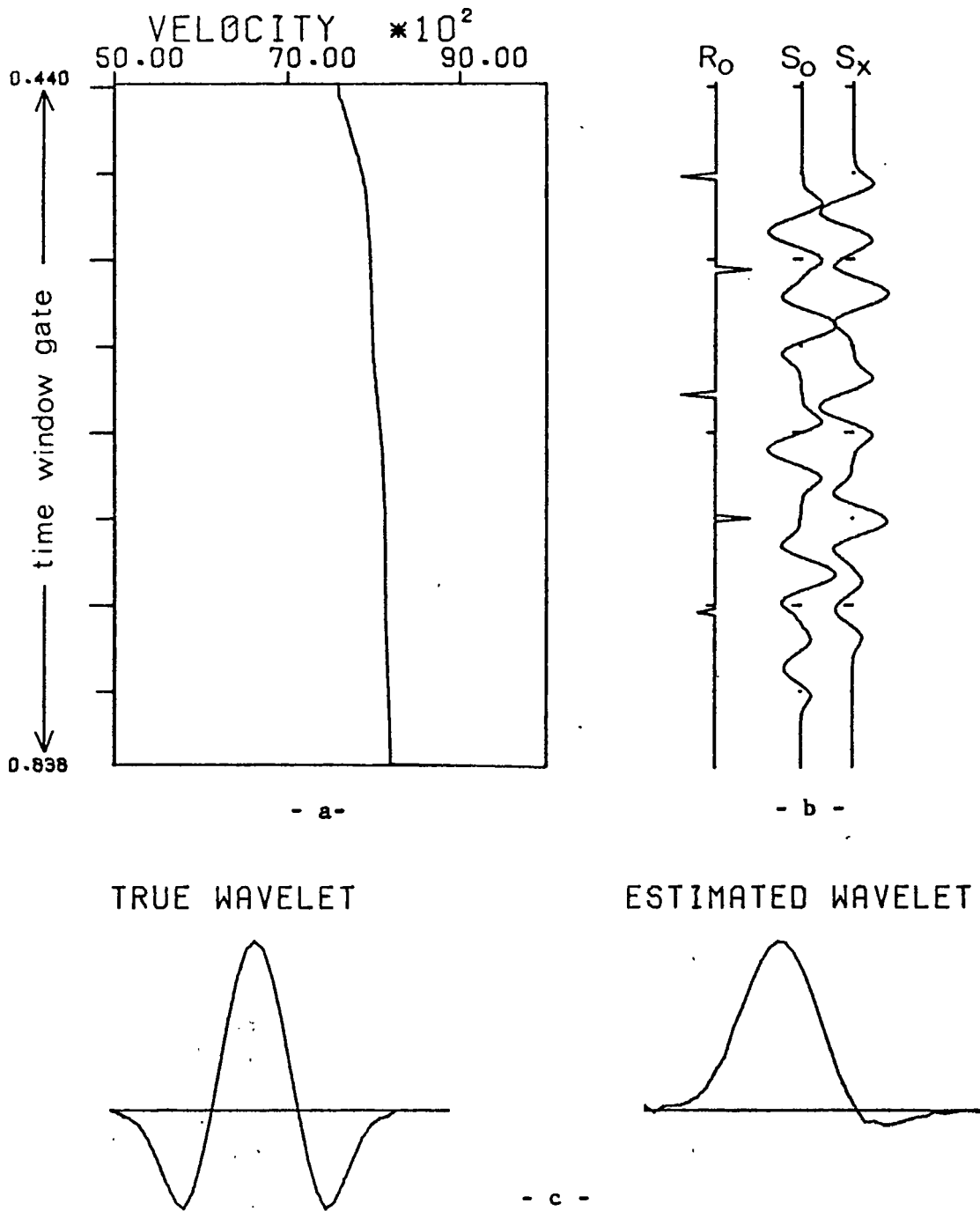


Figure 24. Application of the wavelet extraction method to an unstable model. (a) The average velocity function. (b) The actual reflectivity function, the trace at zero offset and at 2000 ft. (c) The true wavelet and the estimated wavelet after 100 iterations.

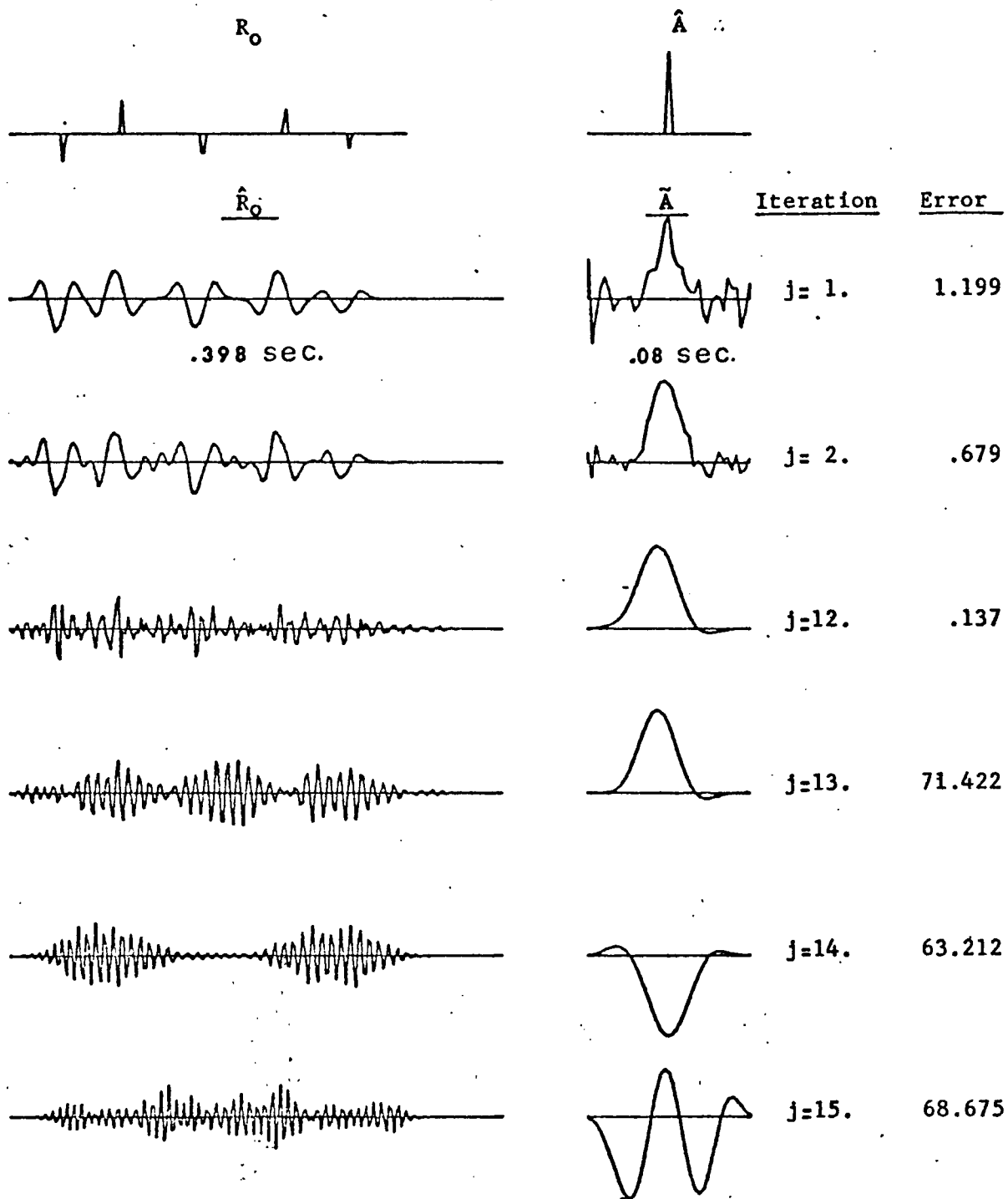


Figure 25. Outputs at various steps of the wavelet extraction method. After 12 iterations the system becomes unstable.

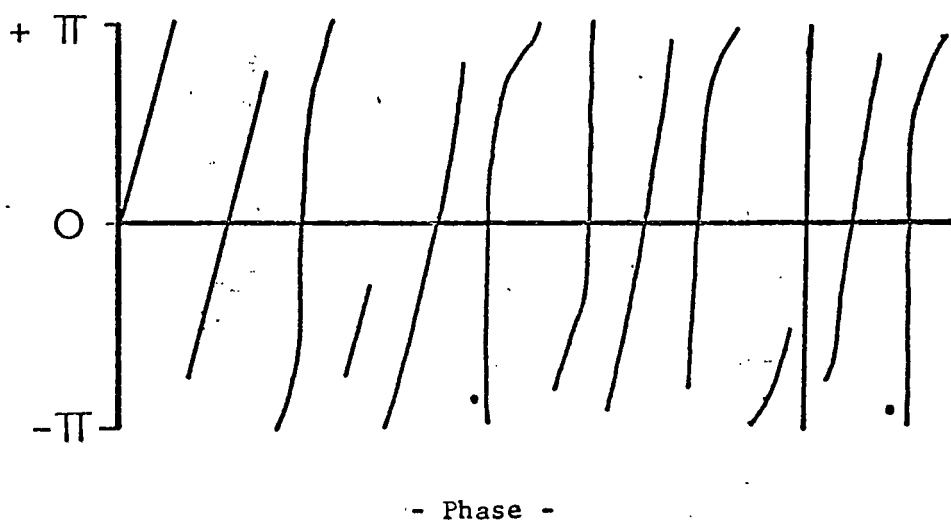
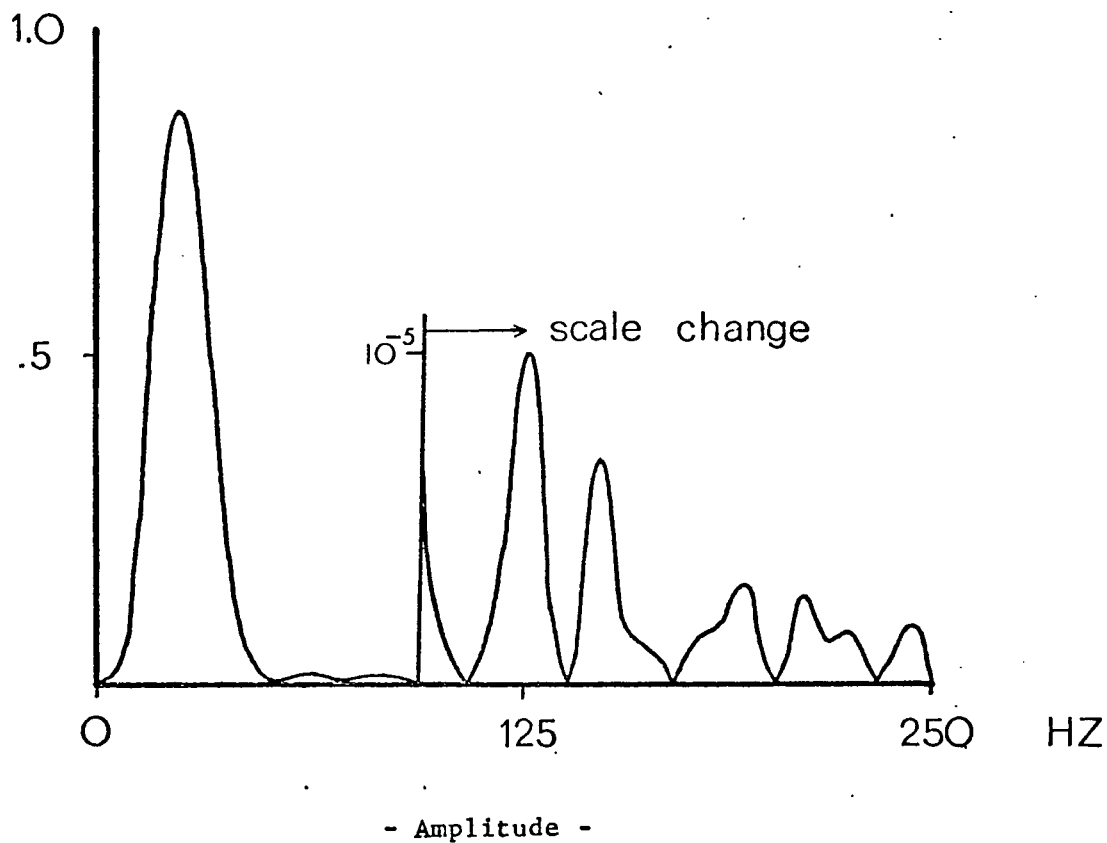


Figure 26. Amplitude and Phase spectra of the true wavelet used in the unstable model.

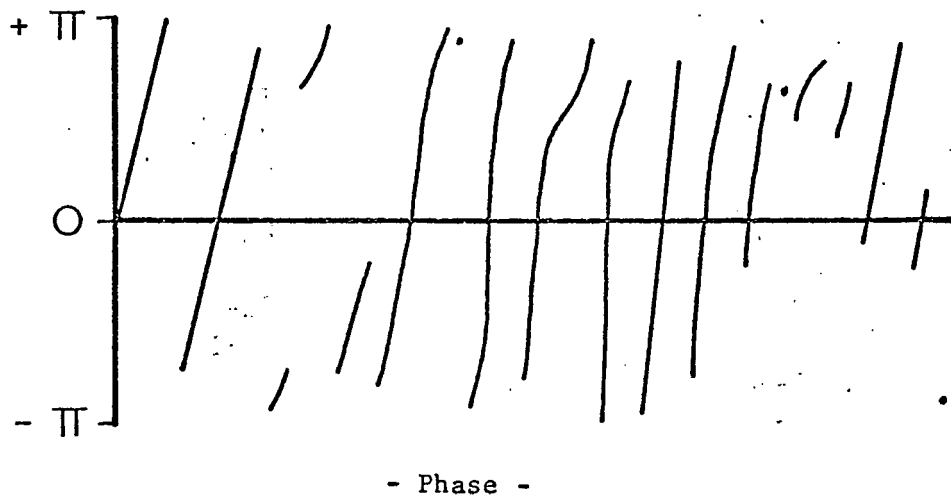
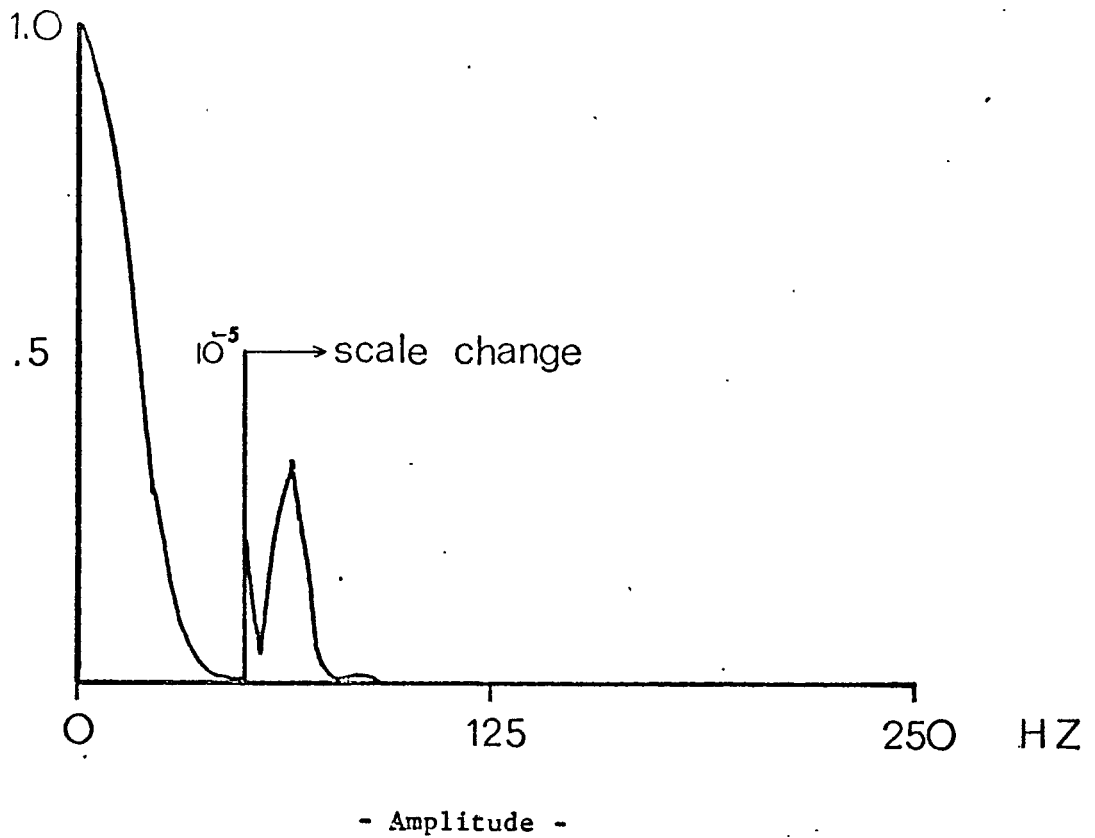


Figure 27. Amplitude and Phase spectra of the estimated wavelet one step before the instability.

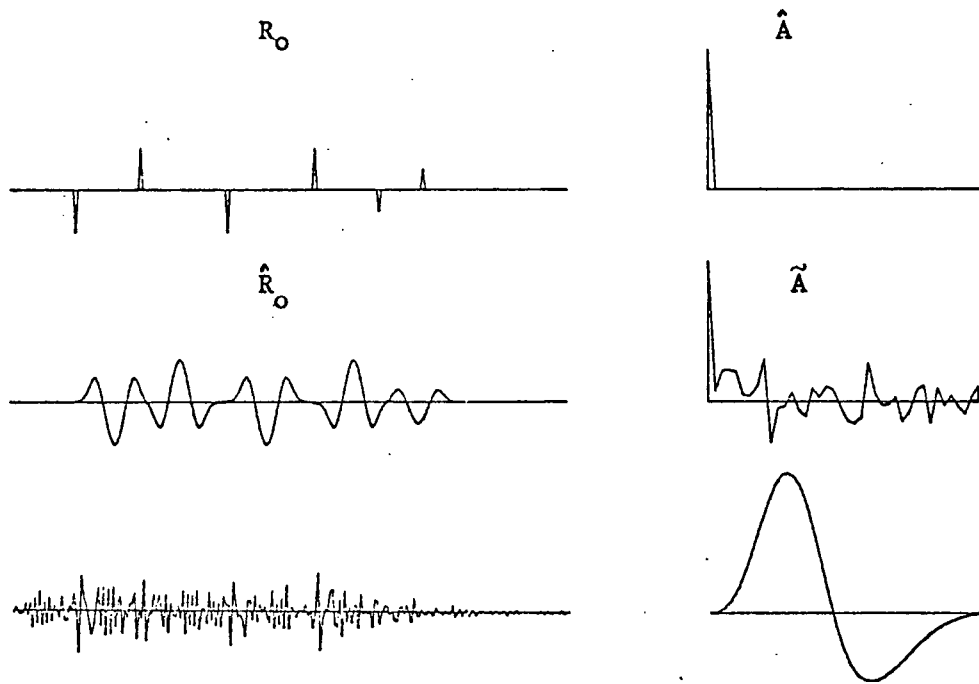


Figure 28. Output at various steps of the wavelet extraction method. The spike on the initial estimate is at time zero.

CONCLUSIONS

Wavelet Compression Technique

Relative to the general problem of deconvolution and seismic interpretation, the wavelet compression technique does not give the answer for all the problems of seismic prospecting. It is definitely a particular tool that could be applied in areas where reflections are good and where an increase in resolution is desired. Specific examples for application are: the enhancement of detail in searching for stratigraphic features and increased definition of the limits of a producing horizon.

Wavelet Extraction Technique

It is a deconvolution method which makes use of the velocity function and offset distance, and does not require any assumption about the shape of the seismic wavelet or restriction on the reflectivity function. When the velocity function is known, the system attempts to recover the exact reflectivity function and the exact seismic wavelet.

For particular situations the system becomes unstable and a vigilant routine must be incorporated into the algorithm in order to avoid this problem. The deconvolution process can be stabilized by different ways and the simplest one is the addition of white noise in the power spectrum of the estimated wavelet.

As the method does not require any mathematical or geological assumptions, it is indicated for use in areas where the velocity function is well known in order to obtain

the exact shape of the best seismic wavelet.

The seismic noise is always present on the field record and can be compensated by using the system for more than two traces. It is not difficult to expand the algorithm for more traces and get a noise reduction.

REFERENCES

- Robinson, E. A., and Treitel, S., 1967, Principles of Digital Wiener Filtering. Geophysical Prospecting, Vol. 15, p. 311-333.
- Sengbush, R. L., Lawrance, P. L., McDonald, F. J., 1961, Interpretation of Synthetic Seismograms. Geophysics, Vol. 26, p. 138-157.
- Treitel, S., and Robinson, E. A., 1966, The Design of High-Resolution Digital Filters, IEEE Transactions on Geoscience Electronics, Vol. GE-4, No. 1.